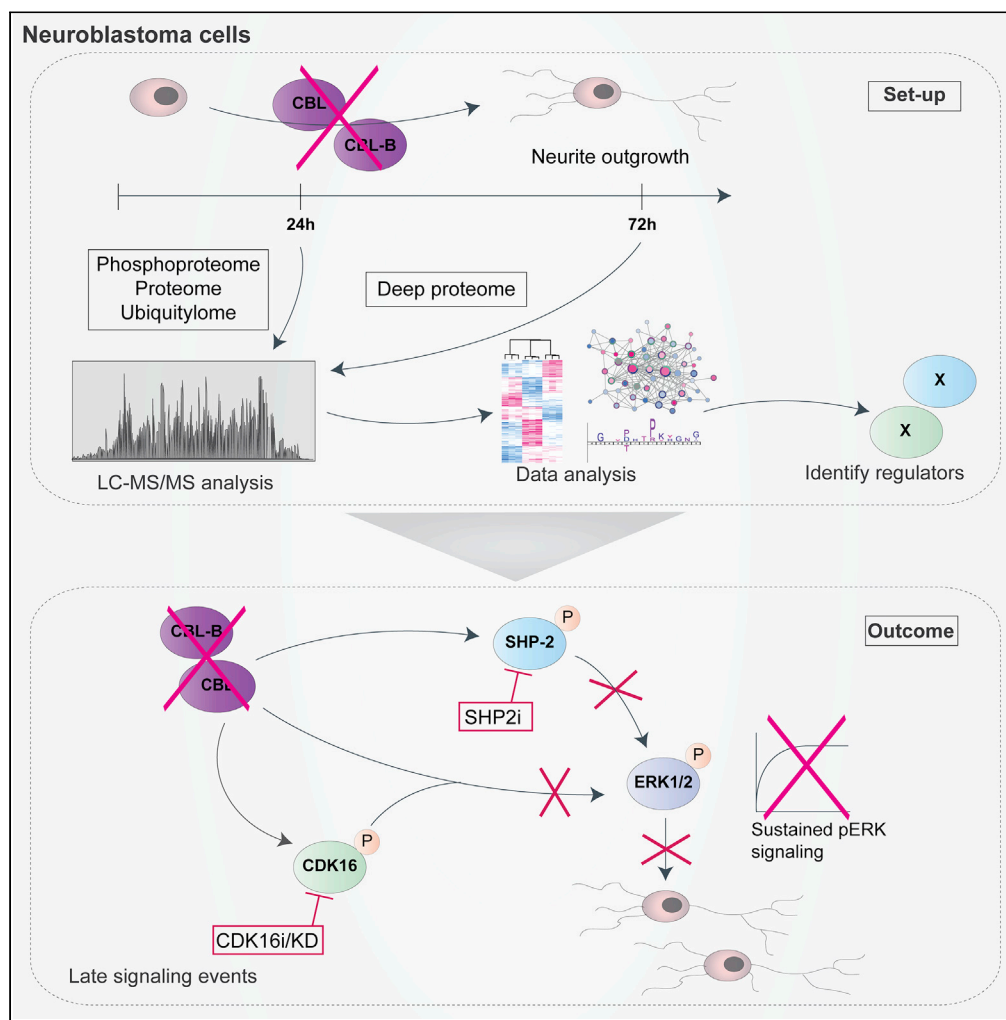


Article

Proteomic investigation of Cbl and Cbl-b in neuroblastoma cell differentiation highlights roles for SHP-2 and CDK16



Anna-Kathrine Pedersen, Anamarija Pfeiffer, Gopal Karemore, ..., Blagoy Blagoev, Chiara Francavilla, Jesper V. Olsen

chiara.francavilla@manchester.ac.uk (C.F.)
jesper.olsen@cpr.ku.dk (J.V.O.)

Highlights
Multi-layered proteomics captures cellular changes induced by Cbl/Cbl-b depletion

SHP-2 and CDK16 protein and phosphorylation levels increase upon Cbl/Cbl-b depletion

SHP-2 and CDK16 regulate phospho-ERK and neurite outgrowth in neuroblastoma cells

Inhibition of SHP-2 or CDK16 reverts Cbl/Cbl-b knockdown effects on differentiation

Pedersen et al., iScience 24, 102321
April 23, 2021 © 2021 The Author(s).
<https://doi.org/10.1016/j.isci.2021.102321>

Article

Proteomic investigation of Cbl and Cbl-b in neuroblastoma cell differentiation highlights roles for SHP-2 and CDK16

Anna-Kathrine Pedersen,¹ Anamarija Pfeiffer,¹ Gopal Karemore,^{1,4} Vyacheslav Akimov,² Dorte B. Bekker-Jensen,¹ Blagoy Blagoev,² Chiara Francavilla,^{3,*} and Jesper V. Olsen^{1,5,*}

SUMMARY

Neuroblastoma is a highly heterogeneous embryonal solid tumor of the sympathetic nervous system. As some tumors can be treated to undergo differentiation, investigating this process can guide differentiation-based therapies of neuroblastoma. Here, we studied the role of E3 ubiquitin ligases Cbl and Cbl-b in regulation of long-term signaling responses associated with extracellular signal-regulated kinase phosphorylation and neurite outgrowth, a morphological marker of neuroblastoma cell differentiation. Using quantitative mass spectrometry (MS)-based proteomics, we analyzed how the neuroblastoma cell line proteome, phosphoproteome, and ubiquitylome were affected by Cbl and Cbl-b depletion. To quantitatively assess neurite outgrowth, we developed a high-throughput microscopy assay that was applied in combination with inhibitor studies to pinpoint signaling underlying neurite outgrowth and to functionally validate proteins identified in the MS data sets. Using this combined approach, we identified a role for SHP-2 and CDK16 in Cbl/Cbl-b-dependent regulation of extracellular signal-regulated kinase phosphorylation and neurite outgrowth, highlighting their involvement in neuroblastoma cell differentiation.

INTRODUCTION

Neuroblastoma is the most common extracranial tumor in childhood and accounts for around 15% of pediatric cancer mortality (Johnsen et al., 2018; Matthay et al., 2016; Ratner et al., 2016). Neuroblastoma is an embryonal solid tumor arising in the developing sympathetic nervous system from cells of the neural crest, and tumor development is associated with failed neuronal differentiation. This disease is characterized by high heterogeneity, encompassing tumors with a high degree of variability in biological characteristics and clinical behaviors. Thus, tumors range from highly malignant and therapeutically resistant to tumors that spontaneously regress or differentiate (Ratner et al., 2016). Risk stratification (based on the International Neuroblastoma Risk Group [INRG] classification system) of patients for targeted therapy has reduced treatment load for low- and intermediate-risk patient groups for whom outcomes are excellent, while patients with high-risk disease are subjected to extensive treatment regimes. Yet, patient survival for high-risk neuroblastoma remains below 50% (Ambros et al., 2009; Cohn et al., 2009; Irwin and Park, 2015; Matthay et al., 2016). Survival is correlated with the level of tumor differentiation; thus, patients with more well-differentiated tumors have a more favorable outcome (Fredlund et al., 2008). Accordingly, differentiation therapy is an attractive strategy for neuroblastoma. Treatment with retinoic acid (RA) has been shown to induce neuroblastoma cell differentiation to a more mature neuronal state, and RA has become part of the standard treatment regime for patients with high-risk neuroblastoma (Johnsen et al., 2018; Matthay et al., 2009; Ratner et al., 2016). However, the exact mechanism of neuroblastoma differentiation remains an enigma, warranting further research and increased understanding of the signaling pathways underlying this process, as this can potentially lead to development of new and improved differentiation therapies and reveal new biomarkers.

The development of neuroblastoma can be seen as a consequence of failed neural crest cell differentiation. Different chemical agents and growth factors have been found to induce neuroblastoma cell differentiation *in vitro*, and receptor tyrosine kinase (RTK) signaling is involved in mediating this process (Edsjö et al.,

¹Proteomics Program, Novo Nordisk Foundation Center for Protein Research, Faculty of Health and Medical Sciences, University of Copenhagen, Blegdamsvej 3B, 2200 Copenhagen, Denmark

²Department of Biochemistry and Molecular Biology, University of Southern Denmark, 5230 Odense, Denmark

³Division of Molecular and Cellular Functions, School of Biological Sciences, Faculty of Biology, Medicine and Health, University of Manchester, Manchester M13 9PL, UK

⁴Present address: Modeling and Predictive Technologies, Novo Nordisk A/S, 2760 Måløv, Denmark

⁵Lead contact

*Correspondence: chiara.francavilla@manchester.ac.uk (C.F.), jesper.olsen@cpr.ku.dk (J.V.O.)

<https://doi.org/10.1016/j.isci.2021.102321>



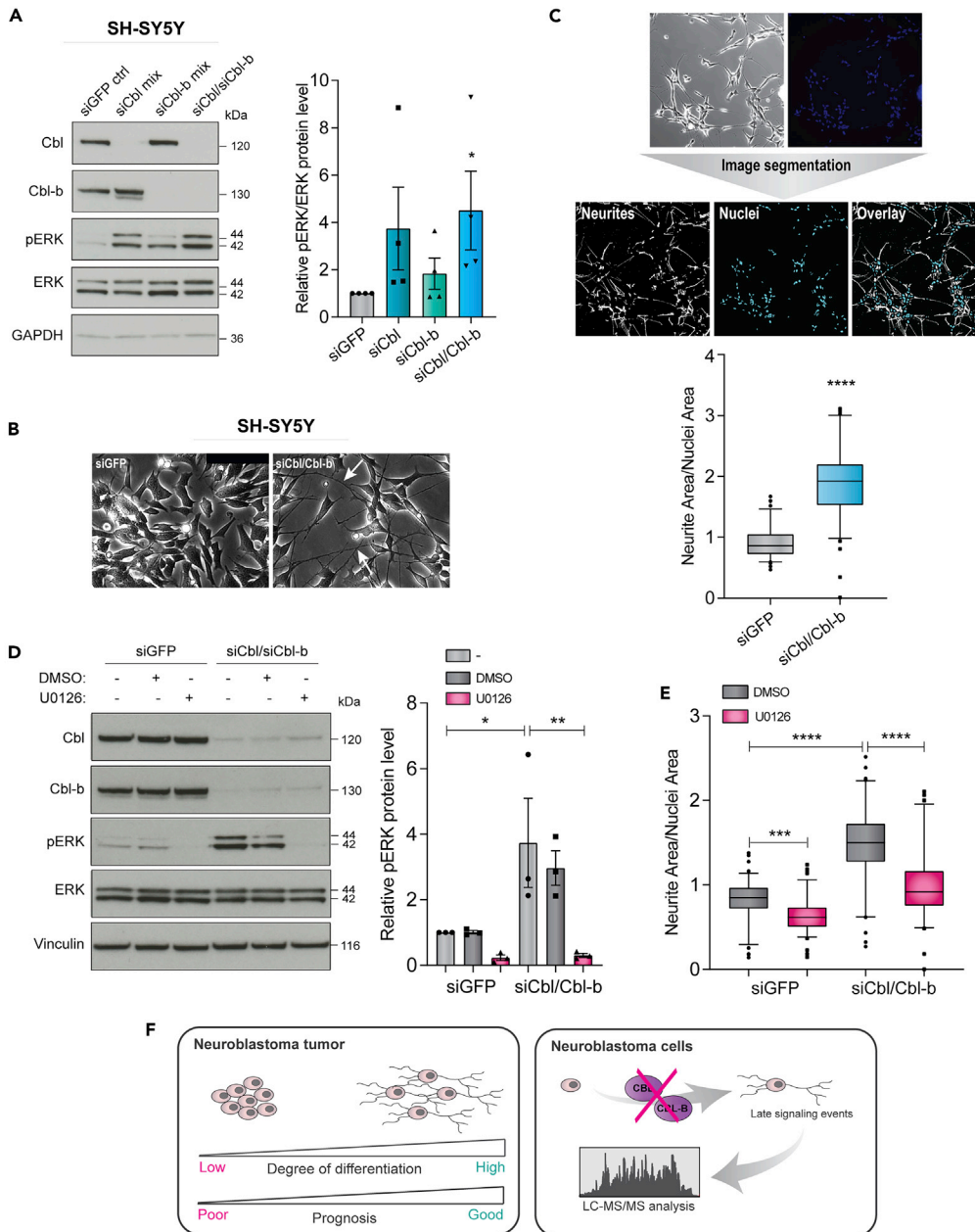


Figure 1. Cbl and Cbl-b regulate SH-SY5Y neuroblastoma cell differentiation by decreasing ERK phosphorylation levels and inhibiting neurite outgrowth

(A–E) SH-SY5Y cells were treated with siRNA (as indicated) for 48–72 hr.

(A) Lysates were subjected to immunoblotting (left panel) with antibodies against phospho-ERK/ERK or Cbl/Cbl-b. Right panel shows quantification relative to siGFP control (n = 4).

(B) Representative images of siGFP and siCbl/Cbl-b-treated cells for neurite outgrowth (indicated by white arrows) visualization (scale bar, 50 μ m).

(C) Representative raw and segmented images of Cbl/Cbl-b knockdown SH-SY5Y cells. Segmented images (bottom panel) show neurites (white) and nuclei (cyan). Neurites and nuclei were quantified by “Neurite Outgrowth Quantification” software.

(D) Immunoblotting (left panel) detecting indicated proteins in lysates of SH-SY5Y treated with Cbl/Cbl-b siRNA in conjunction with U0126 and quantification (right panel) relative to siGFP control.

(E) Corresponding quantification of neurite outgrowth.

Figure 1. Continued

(F) Graphical model of neuroblastoma differentiation and study design. Data in bar graphs are shown as means \pm SEM and in boxplots as median with 95% confidence interval (CI) and representative of $n = 3$ independent experiments. *, **, *** and **** indicate $p < 0.05$, 0.01, 0.001, and < 0.0001 , respectively, compared to the corresponding control determined by one-sample t test (A), t test (C), or one-way ANOVA (D and E).

2007). Neurotrophins and their cognate receptors, belonging to the tropomyosin-related kinase family of RTKs, have central roles in the development and maintenance of the nervous system, and neuroblastoma cells expressing tropomyosin-related kinase A (TrkA) have been shown to undergo differentiation in response to stimulation by its high-affinity ligand, nerve growth factor (NGF). Accordingly, high expression of TrkA is associated with low-stage tumors and a good prognosis (Brodeur and Bagatell, 2014; Edsjö et al., 2007; Mohlin et al., 2011). Signaling from RTKs is tightly regulated by a number of cellular mechanisms including ubiquitylation, internalization, and receptor degradation/recycling mediated by E3 ubiquitin ligases, such as the casitas B-lineage lymphoma protein, Cbl. The Cbl protein family consists of three members: c-Cbl (referred to as Cbl), Cbl-b, and Cbl-3. Cbl proteins are really interesting new gene (RING)-type E3 ubiquitin ligases, which can bind tyrosine-phosphorylated substrates through their tyrosine-kinase-binding domain to mediate ubiquitylation via an E2 ubiquitin-conjugating enzyme bound to the RING finger (Cooper et al., 2015; Thien and Langdon, 2001). Thus, Cbl proteins can specifically direct ubiquitylation of activated RTKs to negatively regulate signaling as it has been shown for a number of RTKs including epidermal growth factor receptor (EGFR), anaplastic lymphoma kinase (ALK), and TrkA (Ettenberg et al., 2001; Mazot et al., 2012; Soubeyran et al., 2002; Takahashi et al., 2011). In addition, the C-terminal regions of Cbl and Cbl-b contain phosphorylation sites and proline-rich regions, through which other adapter proteins can bind and thereby positively regulate signaling pathways by functioning as signaling scaffolds (Cooper et al., 2015; Thien and Langdon, 2001). We have previously identified a role for Cbl-b as a negative regulator of NGF-TrkA signaling in neuroblastoma cells and found that depletion of Cbl and Cbl-b was associated with induction of neurite outgrowth, a morphological marker of neuroblastoma differentiation (Emdal et al., 2015). The aim of the present study was to elucidate the general role of Cbl proteins in regulating RTK signaling and neurite outgrowth in neuroblastoma cells and to identify components of the signaling responses underlying these processes. We applied mass spectrometry (MS)-based quantitative proteomics to obtain an unbiased global view of Cbl-dependent cell signaling pathways in neuroblastoma cells. Analyzing multiple layers of signaling networks including the regulation of proteins and their post-translational modifications (PTMs) by MS-based quantitative proteomics can provide detailed information on cellular responses and reveal implicated molecular mechanisms (Emdal et al., 2018; Francavilla et al., 2013, 2016; Reckel et al., 2017). To gain insights into the roles of Cbl and Cbl-b in the regulation of neurite outgrowth, we investigated the global changes in the proteome, ubiquitylome, and phosphoproteome of Cbl protein-depleted neuroblastoma cells. This multi-layered data set revealed players involved in neuroblastoma cell differentiation and identified roles for signaling proteins insulin-like growth factor 1 receptor (IGF1R), SH2 domain-containing protein tyrosine phosphatase-2 (SHP-2) and cyclin-dependent kinase 16 (CDK16) in Cbl-dependent regulation of neuroblastoma cell function.

RESULTS**E3 ubiquitin ligases Cbl and Cbl-b regulate neurite outgrowth in neuroblastoma cells in an ERK-dependent manner**

To study the roles of the closely related E3 ligases Cbl and Cbl-b in signaling and differentiation of neuroblastoma cells, we initially employed a panel of three neuroblastoma cell lines, namely SH-SY5Y, NB1, and IMR-32. These were selected based on their ability to form cellular projections referred to as neurite outgrowths, a morphological marker of cell differentiation, in response to different stimuli (Halder et al., 2015; Nishimura et al., 1995; Pålman et al., 1995; Rettig et al., 2015). Furthermore, these cell lines express different combinations of oncogenes known to be important for neuroblastoma development and progression, such as amplified MYCN and mutated or amplified ALK (Cheung and Dyer, 2013; Emdal et al., 2018; Matthay et al., 2016) (Figure S1A). To disrupt the function of Cbl and/or Cbl-b, we used small interfering RNA (siRNA)-based knockdown and found by microscopy-based visual inspection that depletion of both induced increased neurite outgrowth in all cell lines, however, less evident in IMR-32. In addition to this phenotypic change, we saw a concomitant increase in extracellular signal-regulated kinase (ERK) phosphorylation upon knockdown of Cbl E3 ligases (Figures 1A, 1B, and S1B–S1E). This is in accordance with the important role of activated ERK in cellular differentiation and neurite outgrowth and supports previous findings (Emdal et al., 2015; Grewal et al., 1999; Robinson et al., 1998). Thus, we applied neurite outgrowth

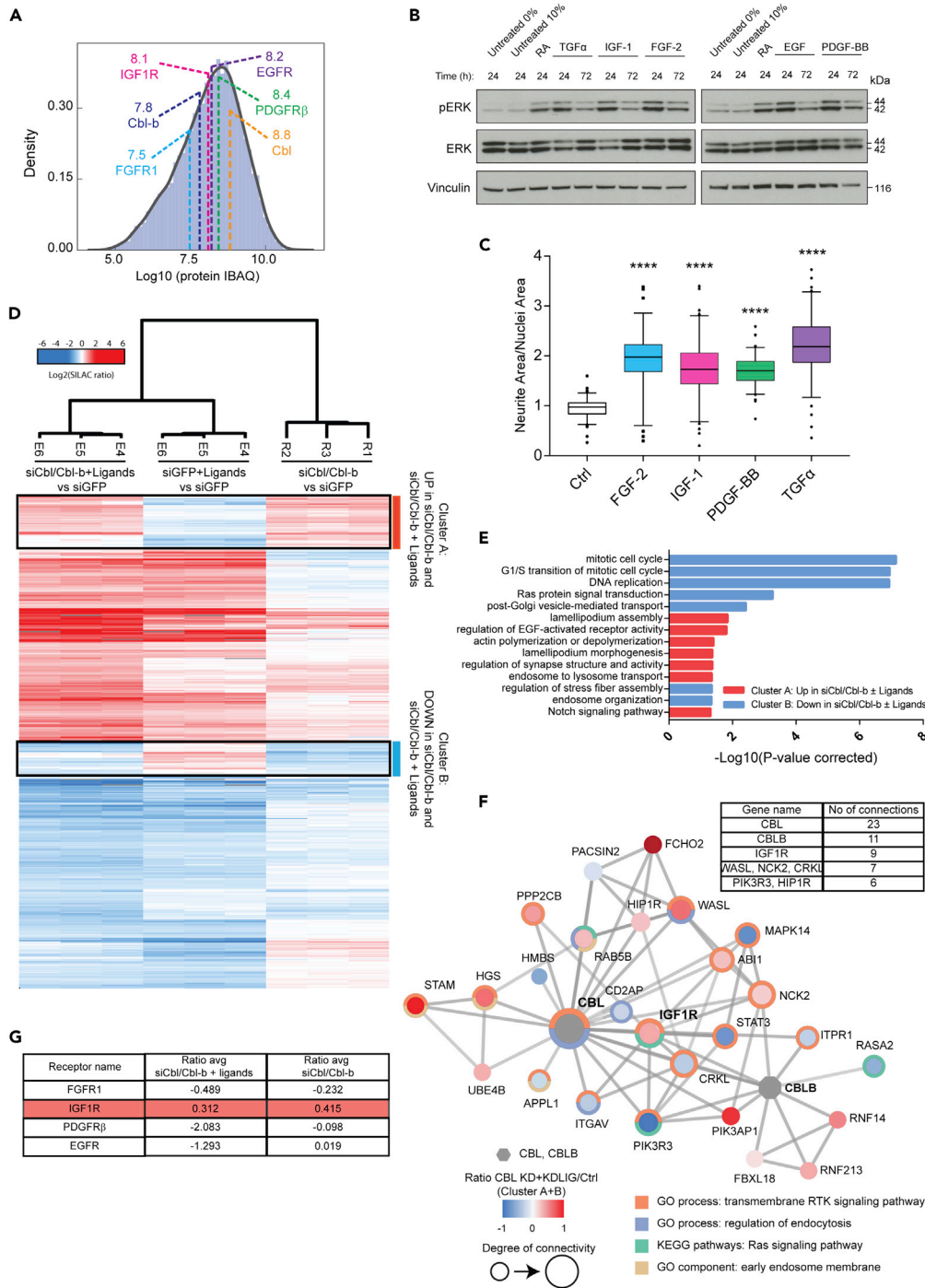


Figure 2. Deep proteome analysis to study the impact of Cbl/Cbl-b on long-term RTK signaling responses in SH-SY5Y cells

(A) Density analysis of protein abundances (IBAQ) in SH-SY5Y cells highlighting Cbl/Cbl-b and RTKs, shown with their corresponding IBAQ values (Log_{10}).

(B) Immunoblotting for phospho-ERK of lysates from SH-SY5Y cells stimulated with FGF-2, IGF-1, PDGF-BB, or TGF α (or EGF). RA was used as a positive control.

(C) Neurite outgrowth quantification of cells exposed to the same conditions as in (B). Data are shown as medians with 95% CI. **** indicates $p < 0.0001$ (one-way ANOVA) compared to the control. Data are representative of $n = 3$ independent experiments.

Figure 2. Continued

(D) Hierarchical clustering of proteins with significantly regulated abundance (ANOVA) in response to treatment with Cbl/Cbl-b siRNA (72 hr) and/or RTK ligand cocktail (FGF-2, IGF-1, PDGF-BB, and TGF α ; 48 hr). The two clusters selected for further analyses are highlighted. Data are presented with log₂ SILAC ratios all relative to siGFP control.

(E) Bar graph illustrating significantly overrepresented GO terms for biological process (GOBP) for cluster A (red) and B (blue).

(F) Functional network analysis of proteins in clusters A and B, displaying first degree connections of Cbl and Cbl-b (gray). Node color indicates regulation on protein level and surrounding colored circles indicate enriched GO terms and KEGG pathways (see legend). The table summarizes the number of connections for the most connected proteins.

(G) Table summarizing average ratios from the proteome data (relative to the siGFP control) for the RTK panel.

in combination with increased levels of ERK phosphorylation as a proxy for neuroblastoma cell differentiation throughout this study. Importantly, we found that the magnitude and robustness of the differentiation response was increased by simultaneous depletion of Cbl and Cbl-b compared to depletion of individual proteins (Figures 1A, 1B, and S1B–S1E). The magnitude of the response varied between cell lines, with IMR-32 being the least responsive to Cbl/Cbl-b depletion (Figures S1C and S1E) and SH-SY5Y cells displaying the largest increase in ERK phosphorylation levels, as well as the most obvious change in morphological phenotype. Thus, we chose SH-SY5Y as the model system for further analysis of the role of Cbl/Cbl-b in neuroblastoma cell differentiation. To validate the specificity of the effects observed upon Cbl/Cbl-b knockdown, we depleted both Cbl and Cbl-b individually in SH-SY5Y using three different siRNAs (S1, S2, and S3) against each protein, as well as two different pools (pooling either S1 or S3) to deplete Cbl and Cbl-b simultaneously. Overall, these results confirmed, for all tested sequences, that knockdown of Cbl proteins leads to increased ERK phosphorylation and increased neurite outgrowth and that this response is amplified by dual depletion of both Cbl and Cbl-b (Figures S1F and S1G). Since RA is an established treatment used for differentiation therapy of patients with neuroblastoma (Matthay et al., 2009), we applied RA treatment as a positive control to compare with our experimental approach. Accordingly, RA treatment over a time course of 24–120 hr caused increased ERK phosphorylation and simultaneously enhanced neurite outgrowth (Figures S1H and S1I), thus validating our system and approach to study neuroblastoma differentiation (Påhlman et al., 1984).

To accurately measure and quantify neurite outgrowth in an unbiased manner from a large number of cells across conditions, we utilized a ScanR fully automated screening microscope and developed a MATLAB-based “Neurite Outgrowth Quantification” software tool (see workflow; Figure S1J). To avoid harsh treatments of the cells, we developed the tool for live-cell imaging and used Hoechst staining to visualize nuclei. Figure 1C depicts a comparison between raw and segmented images. Using this setup, we validated the visually observed increase in neurite outgrowth induced by Cbl/Cbl-b depletion and RA treatment in SH-SY5Y in an unbiased and quantifiable manner (Figures 1C and S1K).

To assess whether ERK activity played an essential role in the differentiation of the SH-SY5Y cells induced by Cbl/Cbl-b depletion, we combined siRNA-mediated knockdown with inhibition of mitogen-activated protein kinase kinase (MEK) by using the small molecule inhibitor U0126. We found that inhibiting MEK activation abolished ERK phosphorylation (Figure 1D) and indeed, inhibition of ERK activation, correlated with a significant decrease in knockdown-induced neurite outgrowth (Figure 1E). Thus, mitogen-activated protein kinase (MAPK) cascade activity is crucial for the induction of neurite outgrowth upon Cbl/Cbl-b depletion, further validating our approach to use phospho-ERK as a marker of neuroblastoma cell differentiation. Accordingly, we applied this model system combined with MS-based proteomics screens to study Cbl-dependent signaling pathways underlying neuroblastoma cell differentiation (Figure 1F).

Proteome changes link Cbl proteins to regulation of long-term cellular responses

The Cbl protein family is known to modulate the signaling response of several RTKs through regulation of RTK internalization and degradation (Mazot et al., 2012; Mohapatra et al., 2013; Rorsman et al., 2016; Shtiegman et al., 2007). Thus, we hypothesized that the effect of Cbl/Cbl-b depletion on ERK phosphorylation and neurite outgrowth may involve altered expression or activity of one or more RTKs. In support of this hypothesis, activation of several different RTKs has previously been shown to induce neurite outgrowth of neuroblastoma cell lines (Lavenius et al., 1994; Motegi et al., 2004). Initially, we identified a panel of prospective RTK candidates in our SH-SY5Y cells by analyzing the distribution of protein abundances in a previously published deep proteome (Bekker-Jensen et al., 2017) (Figure 2A). We selected EGFR, IGF1R, platelet-derived growth factor receptor β (PDGFR β), and fibroblast growth factor receptor 1 (FGFR1) as

RTKs with differential expression levels and stimulated the cells with their respective ligands. Indeed, treatment with FGF-2, IGF-1, PDGF-BB, and transforming growth factor α (TGF α)/EGF, respectively, induced ERK phosphorylation and increased neurite outgrowth upon long-term stimulation over 24–72 hr (Figures 2B and 2C). To identify protein abundance changes associated with Cbl/Cbl-b proteins and neurite outgrowth induction, we performed a large-scale quantitative MS-based proteome analysis of SH-SY5Y cells after 72 hr of Cbl/Cbl-b depletion (Figure S2A). To assess changes in protein levels under both basal as well as conditions of increased RTK activation, we included siGFP control and siCbl/Cbl-b conditions stimulated with a “ligand cocktail” mixture of RTK ligands FGF-2, IGF-1, PDGF-BB, and TGF α . For quantitative comparison between conditions, we applied a double and triple SILAC (stable isotope labeling by amino acids in cell culture)-based setup combined with nanoflow high-performance liquid chromatography-tandem mass spectrometry (LC-MS/MS) and analyzed each experiment in triplicates (Figure S2A). Using our established deep proteome approach (Bekker-Jensen et al., 2017), we identified and quantified 10,030 proteins with Pearson correlation coefficients of 0.60–0.84 between SILAC replicates of the same condition (Figures S2A–S2C and Table S1). We performed an analysis of variance (ANOVA) statistical test and identified 2980 proteins with significantly changed abundance between the analyzed conditions. Unsupervised hierarchical clustering of the significantly regulated proteins resulted in grouping according to treatment and separated the proteins into six major clusters. To decipher the role of Cbl and Cbl-b, we focused on the proteins specifically upregulated or downregulated for the siCbl/Cbl-b vs. siGFP condition both in the presence and absence of ligand stimulation as represented in cluster A (up for siCbl/Cbl-b and siCbl/Cbl-b + ligands) and cluster B (down in siCbl/Cbl-b and siCbl/Cbl-b + ligands) (Figures 2D and S2B and Table S1). Cbl and Cbl-b displayed the lowest SILAC ratio among the downregulated proteins found in cluster B, serving as a quality control of our knockdown experiment. Gene ontology (GO) enrichment analysis for biological processes revealed that upregulated proteins were associated with functions related to RTK signaling regulation, endosomal transport, and cytoskeletal rearrangements (underlying processes like neurite outgrowth) (Figure 2E). The downregulated proteins were mostly associated with cell cycle and DNA replication, which could correlate with the fact that differentiation is often associated with decreased cell cycle progression (Chu and Cheung, 2003; Veal et al., 2002) (Figure 2E).

A STRING-based functional network of proteins in clusters A and B directly linked to Cbl and Cbl-b revealed that our analysis identified several players connected to Cbl protein biology including IGF1R, which was one of the upregulated proteins most strongly connected to Cbl and Cbl-b (Figure 2F). Notably, IGF1R was identified as the only RTK displaying an upregulated expression level in response to Cbl/Cbl-b depletion, independently of receptor stimulation by exogenously added ligands, as shown in Figure 2G. Thus, we considered that downregulation of IGF1R by Cbl/Cbl-b might contribute to the inhibitory effect on neurite outgrowth. Supporting this concept, we observed that increased activity of IGF1R can induce neurite outgrowth of SH-SY5Y associated with increased phosphorylation of ERK (Figures 2B and 2C), which is in line with previous reports (Kim et al., 1997).

Analysis of global changes in ubiquitylation upon Cbl protein depletion

Cbl and Cbl-b function as E3 ubiquitin ligases, and a major function of ubiquitylation is regulating protein stability and degradation. Thus, we investigated global changes in ubiquitylation events upon depletion of Cbl and Cbl-b and how these correlated with changes in the proteome. We analyzed the ubiquitylome of siCbl/Cbl-b-treated SH-SY5Y cells using a double SILAC-based setup (Figure S3A), with antibody-based enrichment of ubiquitylated peptides performed using UbiSite, which allowed us to strictly enrich for ubiquitylated peptides (Akimov et al., 2018). We identified and quantified 6546 ubiquitylated sites distributed on 2486 proteins. Using a one-sample t test, we found 1560 sites to be significantly regulated, with 437 sites being downregulated by Cbl/Cbl-b knockdown and 1123 being upregulated (Table S2). To assess how changes in ubiquitylation correlated with altered protein expression, we plotted the SILAC ratios of all the 1560 regulated ubiquitylated sites against the SILAC ratio of their corresponding protein as found in the 72 hr proteome (Figure S3B, Tables S1 and S2). In addition, we identified 76 shared proteins regulated by siCbl/Cbl-b treatment both on the level of ubiquitylation and in the 72 hr proteome (Figure S3C). Functional network analysis of these 76 proteins revealed several proteins connected to Cbl and Cbl-b displaying different levels of ubiquitylation and protein abundance regulation with only 18 displaying an inverse correlation (Figure S3D). This suggests that the changes in ubiquitylation observed upon Cbl/Cbl-b depletion are implicated in regulation of cell processes in a more complex fashion than simply by altering protein abundance.

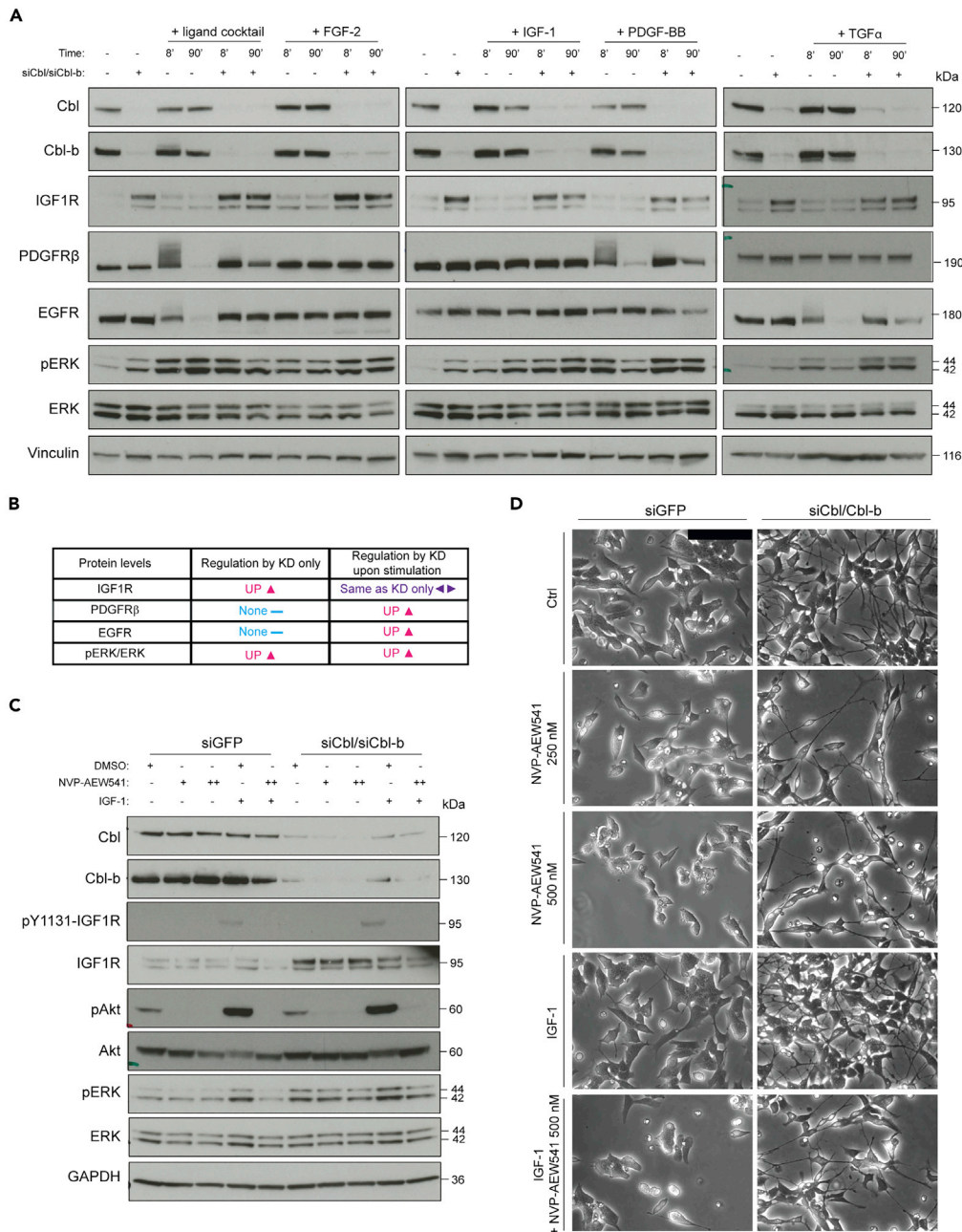


Figure 3. Cbl and Cbl-b regulate MAPK signaling

(A and B) SH-SY5Y cells were treated with control siRNA or siRNAs targeting Cbl and Cbl-b for 48 hr prior to stimulation of RTKs with FGF-2, IGF-1, PDGF-BB, or TGF- α as single ligands or a mix (ligand cocktail) for 8 or 90 min. Lysates were immunoblotted using the indicated antibodies as shown in the representative blots (A) and with findings summarized in table (B).

(C) Immunoblotting of lysates from SH-SY5Y cells treated with siGFP or siCbl/Cbl-b and IGF1R inhibitor (NVP-AEW541; + and ++ indicates 250 or 500 nM, respectively) for 72 hr, detecting the indicated proteins.

(D) Representative images based on the same conditions as in (C) (scale bar, 50 μ m). Data are representative of three independent experiments (n = 3).

Cbl proteins regulate RTK levels and ERK activation in neuroblastoma cells

We validated the changes in protein abundance of the identified RTKs by western blotting and investigated whether potential changes in expression levels correlated with altered magnitude of signaling responses

(e.g. ERK phosphorylation) upon short-term stimulation. Control or Cbl/Cbl-b knockdown cells were stimulated with either the ligand cocktail or FGF-2, IGF-1, PDGF-BB, or TGF α , individually, for 8 and 90 min, respectively. These time points served as a proxy for “maximum” receptor activation (8 min) and receptor internalization/degradation (90 min) (Francavilla et al., 2016). In agreement with the proteome data, results showed that IGF1R protein levels were increased upon depletion of Cbl/Cbl-b compared to siGFP control cells independent of ligand stimulation (Figures 3A and 3B). The levels of both PDGFR β and EGFR increased in Cbl/Cbl-b knockdown cells relative to control after 90 min of receptor stimulation, whereas basal levels were not affected by Cbl/Cbl-b depletion. Correspondingly, levels of receptor ubiquitylation, as indicated by the smeared staining band were apparently decreased after 8 min of stimulation in knockdown cells (Figures 3A and 3B). Changes in receptor levels were persistently associated with similar differences in downstream signaling events as exemplified here by increased levels of phosphorylated ERK, a common converging signaling hub for activated RTKs (Figures 3A and 3B). Furthermore, ERK phosphorylation revealed distinct kinetics of the activated RTKs in these cells. For example, ERK phosphorylation downstream of exogenously activated IGF1R peaked at 90, compared to 8 min under both control and Cbl/Cbl-b knockdown conditions, whereas phospho-ERK levels were dramatically decreased in the presence of Cbl/Cbl-b after 90 min of PDGFR and EGFR activation. These findings together with the proteome data support our hypothesis that IGF1R could be the central RTK implicated in the long-term signaling responses regulating neurite outgrowth and ERK phosphorylation in the SH-SY5Y cells. To further investigate the functional role of IGF1R, we treated the cells with siRNA against Cbl and Cbl-b, while simultaneously inhibiting IGF1R activity using either linsitinib (OSI-906) or NVP-AEW541. While NVP-AEW541 is not approved for clinical use, linsitinib has been in 24 clinical trials; however, trials were discontinued due to suboptimal results. Both inhibitors specifically inhibited IGF1R phosphorylation in response to IGF-1 and abolished Akt phosphorylation, a central mediator of IGF1R signaling, both in stimulated as well as basal conditions. This points to a central role of IGF1R in regulation of Akt signaling in the neuroblastoma cells. Furthermore, inhibitor treatment decreased IGF-1-induced ERK phosphorylation. However, in contrast to our hypothesis, the increase in ERK phosphorylation observed in response to depletion of Cbl and Cbl-b was not noticeably affected by IGF1R inhibition (Figures 3C and S3E). Accordingly, manual visual inspection of cell morphology by phase-contrast microscopy revealed that neurite outgrowth induced by Cbl/Cbl-b depletion was not dependent on IGF1R activity. However, an apparent decrease in cell numbers upon treatment with IGF1R inhibitor, under all conditions including knockdown, was evident despite the sustained ERK activation (Figures 3D and S3F). These findings suggest that IGF1R signaling induces a mitogenic rather than a cell differentiation response in this context. To investigate this, we treated Cbl/Cbl-b knockdown or siGFP control SH-SY5Y cells with increasing doses of the IGF1R inhibitor OSI-906 and performed cell survival assays. These data showed that IGF1R signaling seems to support neuroblastoma cell survival and that Cbl/Cbl-b-knockdown cells were indeed slightly more sensitive toward IGF1R inhibition than control cells, displaying a lower OSI-906 IC50 value (Figure S3G).

Late phospho-signaling analysis reveals potential regulators of the neurite outgrowth response induced by Cbl protein depletion

As Cbl and Cbl-b are implicated in regulation of cellular signaling (Thien and Langdon, 2001), we reasoned that the absence of Cbl proteins might affect the long-term phosphorylation status of several other proteins involved in neurite outgrowth besides ERK. To globally assess changes in phosphorylation levels, we analyzed the phosphoproteome of Cbl/Cbl-b-depleted SH-SY5Y cells. We included an RA-treated condition to represent known differentiation signaling and help detect changes associated with neurite outgrowth. Samples were prepared in triplicates, and lysates were labeled by stable isotope-labeled tandem mass tags (TMTs) 10-plex and mixed prior to phosphopeptide enrichment with TiO₂ beads and separation by offline high-pH reversed-phase fractionation before LC-MS/MS analysis (Figure S4A). We identified and quantified 15,480 phosphorylation sites, of which 12,640 were confidently localized (class I sites) to a specific serine (11,004), threonine (1544), or tyrosine (92) in the peptide sequence (Figures S4B and S4C and Table S3). The sites were distributed on 3439 phosphoproteins, and most peptides were identified as singly phosphorylated (Figures S4B and S4D). Furthermore, fractions of the samples were used for proteome profiling as described in Figure S4A. Hierarchical clustering separated both phosphoproteome and proteome data according to treatment (Figures S4E and S4F). ANOVA statistical testing identified 796 class I sites as being differentially phosphorylated between the three conditions. Hierarchical clustering separated these sites into six main clusters (Figure 4A and Table S3). Sites considered regulated by siCbl/Cbl-b treatment were found by combining clusters 1 and 2 (202 sites upregulated by Cbl/Cbl-b depletion) and clusters 3 and 4 (263 sites downregulated by Cbl/Cbl-b depletion). For RA treatment, we found 305

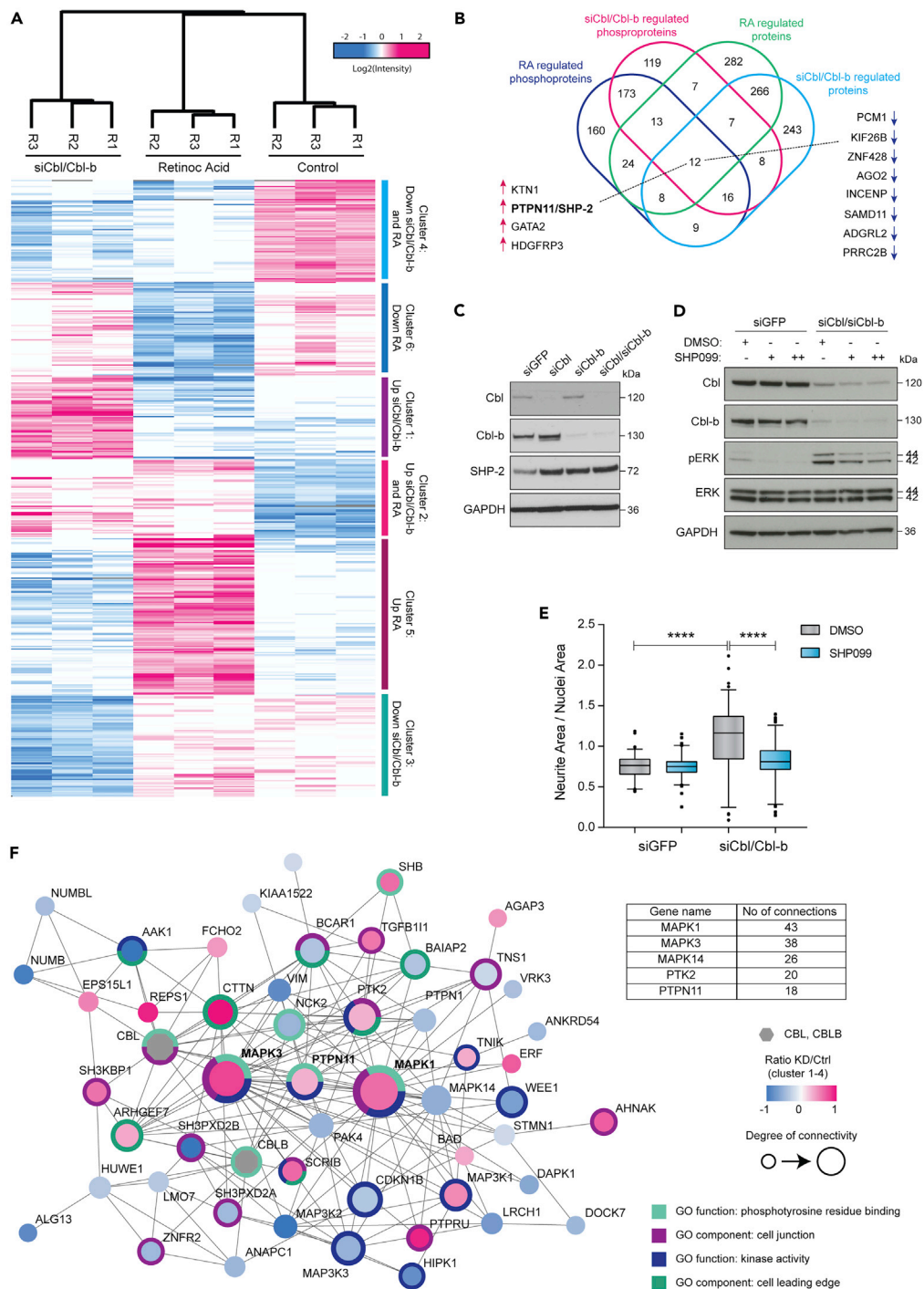


Figure 4. Phosphoproteomics identifies SHP-2 among the regulators of ERK-driven neurite outgrowth

(A) Hierarchical clustering of phosphorylation sites differentially regulated (ANOVA) by treatment with Cbl/Cbl-b siRNA or retinoic acid (RA) for 24 hr. The six identified clusters selected for further analyses are highlighted. Data are presented with \log_2 normalized TMT intensities.

(B) Venn diagram showing the overlap of phosphoproteins and proteins regulated by siCbl/Cbl-b and RA treatment. Common proteins are highlighted with arrows indicating upregulation/downregulation.

(C) Immunoblotting of lysates from SH-SY5Y cells treated with siGFP, siCbl, siCbl-b, or both, detecting the indicated proteins.

Figure 4. Continued

(D) Immunoblotting of lysates from SH-SY5Y cells treated with siGFP or siCbl/Cbl-b and SHP-2 inhibitor (SHP099; + and ++ indicates 5 or 10 μ M, respectively) for 72 hr.

(E) Quantification of neurite outgrowth based on the same conditions as in (D). Data are shown as medians with 95% CI. Data are representative of three independent experiments (n = 3). **** indicates $p < 0.0001$ (one-way ANOVA).

(F) Cluster containing Cbl and Cbl-b (gray) detected by MCL clustering based on functional network analysis of proteins belonging to clusters 1-4. Node color indicates regulation at phosphosite level for knockdown (KD) relative to control. Most significantly overrepresented GO terms are indicated in outer circle and color legend. The table summarizes the number of connections for the most connected proteins.

upregulated sites (clusters 2 and 5) and 253 downregulated sites (clusters 4 and 6). The same analysis was carried out for the proteome (Figure S4G and Table S4). To pursue the idea of potential common regulators of ERK activation and neurite outgrowth, we initially focused on the shared fraction of regulated phosphoproteins and proteins between Cbl/Cbl-b-depleted and RA-treated cells (Figure 4B). A total of 12 proteins were regulated both on the phosphoproteome and protein level of which 4 and 8 were upregulated and downregulated, respectively (see Figure 4B). We reasoned that central protein hubs in the Cbl-dependent network incorporate multilevel signals and are therefore regulated on several proteomic levels (Francavilla et al., 2016). Within the upregulated group, we found the tyrosine phosphatase SHP-2 as an interesting candidate for further investigation. SHP-2 represents a known signaling hub for relaying signals from the cell surface to downstream effectors, has been connected to neurite outgrowth (Chen et al., 2002; Wright et al., 1997), and is a clinically relevant phosphatase considering that 14 phase 1 and phase 2 trials with SHP-2 allosteric inhibitor are currently running. By western blotting, we validated the increased protein levels of SHP-2 upon Cbl/Cbl-b knockdown observed in the proteome data (Figures 4C and 4B/S4G). SHP-2 has previously been linked to neurite outgrowth (Chen et al., 2002; Wright et al., 1997) and is known to be essential for full activation of the RAS/ERK pathway (Chan and Feng, 2007). Thus, we hypothesized that under normal conditions, Cbl proteins inhibit SHP-2 either directly or indirectly, thereby inhibiting ERK phosphorylation and neurite outgrowth. To test this hypothesis, we applied the recently developed first-in-class allosteric SHP-2 inhibitor SHP099 (Chen et al., 2016) to specifically target SHP-2 function in combination with Cbl and Cbl-b depletion and observed decreased levels of siCbl/Cbl-b-induced ERK phosphorylation upon SHP-2 inhibition (Figure 4D). This effect was associated with a relative decrease in the level of neurite outgrowth (Figure 4E). However, we still observed residual levels of ERK phosphorylation in response to Cbl/Cbl-b depletion in the presence of SHP099 (Figure 4D). Thus, we reasoned that the complete regulatory effect on ERK activation and neurite outgrowth mediated by Cbl proteins could not be ascribed to SHP-2-dependent signaling alone. Focusing our analysis on the total number of siCbl/Cbl-b-regulated phosphorylation sites (465), we performed a functional network analysis of phosphoproteins regulated by siCbl/Cbl-b treatment (clusters 1–4), which grouped these into two main clusters. One of these was highly connected to Cbl (and Cbl-b) and with functions in processes such as phosphotyrosine binding and kinase signaling. This cluster was centered on MAPK ERK1/2 as the most connected proteins and contained other proteins linked to MAPK signaling, including SHP-2/PTPN11 (Figure 4F). KEGG (Kyoto Encyclopedia of Genes and Genomes) pathway enrichment analysis of proteins with regulated phosphosites revealed an overrepresentation of proteins associated with e.g. signaling and cytoskeletal rearrangements (focal adhesion) for upregulated sites and cell cycle for downregulated sites (Figure S4H).

The partial effect of SHP-2 inhibition suggests that several interconnected signaling networks are needed to regulate ERK activity and neurite outgrowth and that the Cbl proteins seem to be central signaling hubs underlying this regulation.

CDK16 is implicated in the regulation of ERK phosphorylation and neurite outgrowth in response to Cbl protein knockdown

To identify protein kinases implicated in the Cbl/Cbl-b-dependent effect on neurite outgrowth, we performed a sequence motif analysis (Colaert et al., 2009), which relies on the fact that the specificity of many kinases can be assigned to their preferred consensus sequence surrounding the phosphorylated residue. We focused on the upregulated sites as we expect increased activity of kinases functioning as drivers of this process. By comparing phosphorylation sites exclusively upregulated by Cbl/Cbl-b depletion (cluster 1; Figure 4A) to those exclusively upregulated by RA (cluster 5; Figure 4A), we found a strong preference of sites in cluster 1 for proline in the +1 position relative to the phosphorylated residue (Figure 5A). This observation points to a higher activation of proline-directed kinases in cells depleted of Cbl and Cbl-b.

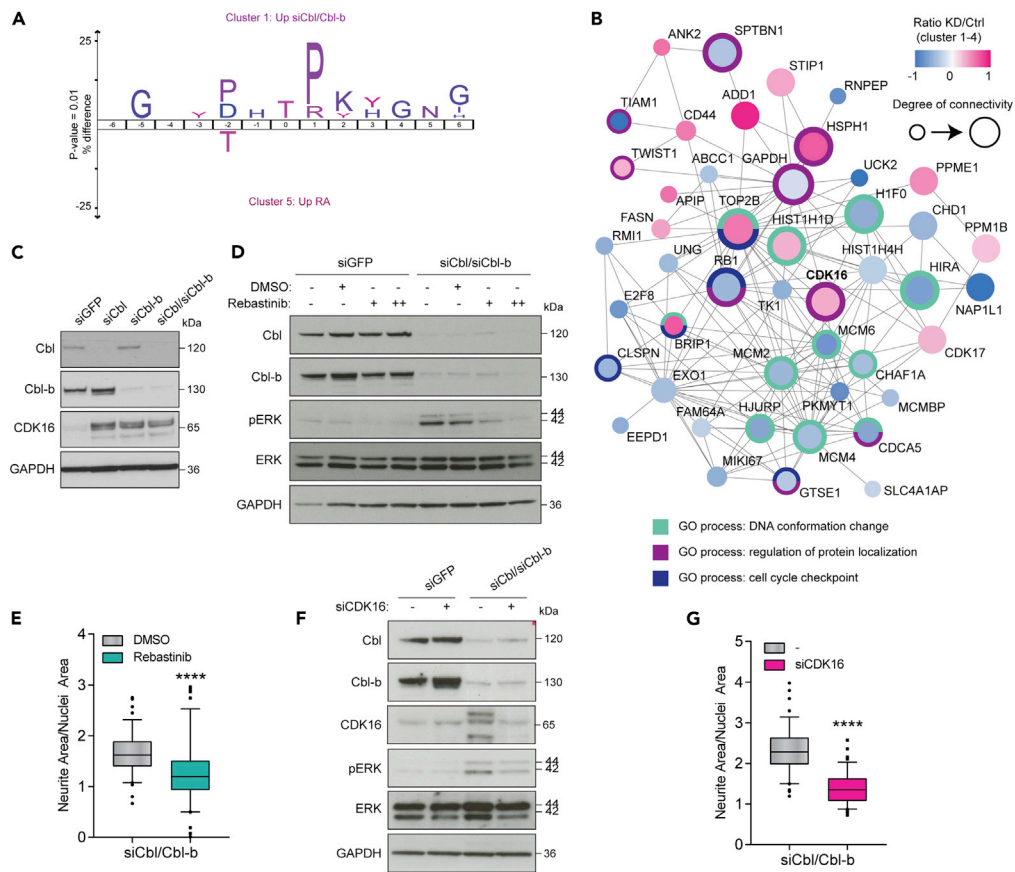


Figure 5. The inhibitory effect of Cbl/Cbl-b on neurite outgrowth depends on CDK16 activity

(A) Sequence motif analysis (IceLogo) of the 6 amino acid residues flanking the regulated phosphorylation site as identified in Figure 4A, cluster 1 (KD-upregulated) compared to cluster 5 (RA-upregulated).
 (B) Second largest cluster detected by MCL clustering based on functional network analysis of proteins belonging to clusters 1-4 from Figure 4A. Node color indicates regulation at phosphosite level for KD relative to control. Most significantly overrepresented GO terms are indicated in outer circle and color legend. CDK16 is highlighted in bold.
 (C) Immunoblotting of lysates from SH-SY5Y cells treated with siGFP, siCbl, siCbl-b, or both, detecting the indicated proteins (same lysates as in Figure 4C).
 (D) Immunoblotting of lysates from SH-SY5Y cells treated with siGFP or siCbl/Cbl-b and CDK16 inhibitor (rebastinib; + and ++ indicates 0.5 or 1 μ M, respectively) for 48–72 hr. Data are representative of three independent experiments (n = 3).
 (E) Representative quantification of neurite outgrowth based on the conditions in (D).
 (F) Immunoblotting of lysates from SH-SY5Y cells treated with siGFP or siCbl/Cbl-b and siCDK16 for 72 hr, using the indicated antibodies.
 (G) Quantification of neurite outgrowth based on the same conditions as in (F). Data in boxplots are shown as medians with 95% CI. Data are representative of two ([E] and [G]) or three (F) independent experiments (n = 2-3). **** indicates $p < 0.0001$ (t test).

The group of well-established proline-directed kinases includes kinase families related to MAPK signaling (such as ERK and p38), glycogen synthase kinase-3 (GSK3), and cyclin-dependent kinases (CDKs).

Among the kinases upregulated in response to Cbl/Cbl-b depletion, we identified the CDK CDK16, as part of the second largest cluster in the functional network analysis (Figure 5B). This cluster contained proteins mostly related to DNA and cell cycle regulation. We found phosphorylation of CDK16 on a regulatory site Ser119 to be exclusively upregulated by Cbl/Cbl-b knockdown (cluster 1 in Figure 4A). Furthermore, the protein levels of CDK16 were also significantly increased by knockdown of Cbl proteins in the 72 hr proteome data set (cluster A in Figure 2D and Table S1). The increase in CDK16 protein levels upon Cbl protein knockdown was subsequently validated by western blotting (Figure 5C). CDK16 is not very well studied but has been linked to different signaling pathways and processes such as exocytosis, spermatogenesis,

autophagy, and neuronal development (Dohmen et al., 2020; Malumbres, 2014; Mokalled et al., 2010). Thus, we considered that this kinase might mediate the siCbl/Cbl-b-dependent effects on ERK and neurite outgrowth. To further investigate the functional role of CDK16 and establish a link to Cbl protein function, we used the pharmacological inhibitor rebastinib, which has been shown to target CDK16 (Dixon-Clarke et al., 2017). We treated the neuroblastoma cells in combination with siCbl/Cbl-b treatment and observed that the effect of Cbl/Cbl-b depletion on ERK phosphorylation was abolished by rebastinib treatment (Figure 5D). This also correlated with an observed decrease in the levels of neurite outgrowth (Figure 5E). Rebastinib is currently in three phase 1 or 2 clinical trials, as combinatorial treatment, and is commonly used to target the tyrosine kinase Abl1. To check for potential effects of other targets, we investigated the protein expression of Abl1 as well as other potential rebastinib off-targets as reported by the supplier. Four of these proteins were not found to be expressed in the SH-SY5Y cells by our deep proteome analysis, while the other five were detected, yet none of these were specifically regulated by Cbl/Cbl-b depletion (Figure 2D; cluster A and B). Src and Lyn, however, were found in the commonly upregulated and downregulated clusters, respectively, displaying large ratios for cocktail ligand stimulation but only very small ratios for Cbl/Cbl-b depletion (Figure S5A). We identified several phosphosites on some of these potential off-targets; however, not a single site on any of the proteins was regulated by Cbl/Cbl-b knockdown (Figure S5A). Overall, we concluded that reported rebastinib off-targets were not responsible for the Cbl protein-dependent effects on ERK regulation and neurite outgrowth in our system. To confirm that rebastinib targeted CDK16 in the neuroblastoma cells, we treated SH-SY5Y cells with rebastinib in a concentration based on the determined IC50 value (Figure S5B) and performed a cellular thermal shift assay (Jafari et al., 2014). Immunoblotting of rebastinib or dimethyl sulfoxide (DMSO)-treated cells for CDK16 revealed increased stability of CDK16 in lysates of cells treated with the inhibitor compared to vehicle (Figure S5C). This indicated that rebastinib binds to CDK16 in SH-SY5Y. To further validate a functional role of CDK16 in ERK phosphorylation and neurite outgrowth, we treated Cbl/Cbl-b-depleted cells with siRNAs targeting CDK16. We observed that treatment with CDK16 siRNAs blocked the siCbl/Cbl-b-induced increase in CDK16 protein and that this correlated with decreased levels of ERK phosphorylation and neurite outgrowth (Figures 5F and 5G). These data align with the results of the rebastinib treatment and support the theory of CDK16 playing a role in the Cbl-mediated effects on ERK phosphorylation and neurite outgrowth in neuroblastoma cells. To examine whether the regulatory role of Cbl and Cbl-b observed in SH-SY5Y could be relevant to neuroblastoma in general, we depleted Cbl and Cbl-b in two other neuroblastoma cell lines, Kelly and NBL-S, to assess the effects on protein levels of CDK16, SHP-2, and IGF1R as well as the effects on ERK phosphorylation and neurite outgrowth. Knockdown of Cbl/Cbl-b in both cell lines resulted in increased levels of CDK16, SHP-2, and IGF1R in line with the data from SH-SY5Y (Figure S5D). This was accompanied by increased phospho-ERK and a trend toward increased neurite outgrowth, although the morphological changes in the phenotype were not as evident as for SH-SY5Y (Figures S5D and S5E). These data suggest a general link between Cbl E3 ligases, CDK16 and SHP-2, and ERK phosphorylation in neuroblastoma.

DISCUSSION

In this study, we investigated the role of Cbl proteins (Cbl and Cbl-b) in regulation of neuroblastoma cell differentiation by using large-scale proteomics analysis of long-term signaling responses in combination with biochemical and functional assays. Through this approach, we identified proteins such as the tyrosine phosphatase SHP-2 and the CDK CDK16 to be involved in Cbl protein-mediated regulation of sustained ERK phosphorylation and neurite outgrowth in SH-SY5Y cells (Figure 6).

This investigation was prompted by our previous discovery that individual Cbl proteins inhibit neurite outgrowth in neuroblastoma cells (Emdal et al., 2015). Initially, we found an increased effect on neurite outgrowth and ERK phosphorylation in neuroblastoma cell lines by simultaneous depletion of Cbl and Cbl-b compared to individual knockdown. An additive effect of depleting both Cbl and Cbl-b has also been shown for Cbl protein-mediated regulation of ubiquitylation and activation of RTKs, exemplified by PDGFR β (Rorsman et al., 2016).

The role of Cbl proteins in activation-induced regulation of RTK stability and signaling is well established (Ettenberg et al., 2001; Miyake et al., 1998; Petrelli et al., 2002; Wong et al., 2002; Yokouchi et al., 1999); thus, our initial hypothesis focused on the involvement of RTKs in Cbl protein-dependent regulation of sustained ERK phosphorylation and neurite outgrowth. We were intrigued to find that basal IGF1R protein levels were increased upon Cbl depletion; however, inhibition of IGF1R activity did not abolish the increase in ERK

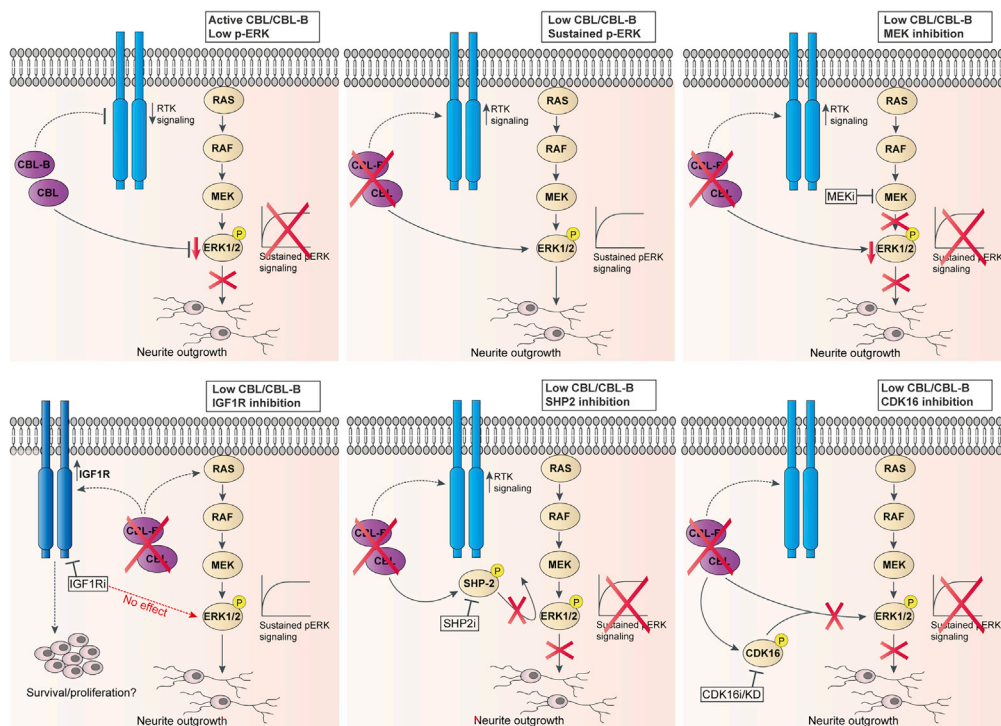


Figure 6. Schematic of the role of Cbl and Cbl-b and associated signaling proteins in regulation of ERK phosphorylation and neurite outgrowth in neuroblastoma cells

Models summarizing the role of Cbl and Cbl-b in negative regulation of ERK phosphorylation and neurite outgrowth in the SH-SY5Y neuroblastoma cells. The schematics illustrate the identified signaling proteins and how inhibition of these proteins revealed their implication in Cbl/Cbl-b-dependent regulation of ERK phosphorylation and neurite outgrowth.

phosphorylation and neurite outgrowth (Figure 6). This was observed despite an increase in neurite outgrowth upon IGF1R ligand-induced activation. Cbl proteins have previously been found to regulate IGF1R ubiquitylation and turnover in response to ligand stimulation (Li et al., 2014; Sehat et al., 2008). The increased IGF1R levels upon Cbl knockdown could potentially be coupled with increased neuroblastoma cell viability or proliferation, as we do observe a slightly higher dependency on IGF1R for cell survival of Cbl/Cbl-b-depleted SH-SY5Y cells treated with IGF1R inhibitor (Figure S3G). Indeed, IGF1R inhibition has been associated with decreased neuroblastoma cell growth and shown potent anti-tumor effects (Guerreiro et al., 2006; Tanno et al., 2006; Van den Eynden et al., 2018; Zhao et al., 2015). Thus, there could be a rationale for further investigations into the possibilities of combining IGF1R inhibition with differentiation therapy through modulation of Cbl protein signaling networks for the treatment of neuroblastoma.

Through our analysis of global long-term phospho-signaling, we identified the tyrosine phosphatase SHP-2 as upregulated both on phosphosite and protein level in response to Cbl protein depletion and RA treatment. This pointed to a general role of SHP-2 in neuroblastoma cell differentiation. Indeed, this oncogenic phosphatase is implicated in the regulation of RTK signaling responses and neurite outgrowth (Chen et al., 2002; Hanafusa et al., 2004; Perrinjaquet and Iba, 2010; Wright et al., 1997). While inhibition of SHP-2 with the inhibitor SHP099 (Chen et al., 2016) partially reversed the effect of Cbl protein depletion on ERK phosphorylation and neurite outgrowth (Figure 6), the full effects could not be explained by SHP-2 regulation alone. Our phosphoproteome data set also pointed to a potential role of CDK16 in Cbl protein-dependent regulation of neurite outgrowth supported by the 72-hr deep proteome data in which CDK16 was identified as one of the top three most upregulated kinases. We found that inhibition of CDK16 with rebastinib or siRNA-mediated knockdown of CDK16 abolished ERK phosphorylation and neurite outgrowth in response to Cbl protein depletion. CDK16 belongs to the PCTAIRE subfamily of CDKs. CDK16 has previously been connected to neurite outgrowth regulation; thus, siRNA-based knockdown of CDK16 has been shown to disrupt dendrite development as well as neurite outgrowth in primary neuron cultures (Fu et al., 2011; Graeser et al., 2002; Mokalled et al., 2010). Intriguingly, the PCTAIRE family has recently been highlighted

as a significantly understudied CDK group of oncology drug targets (Axtman et al., 2019). Here, we report an association of CDK16 to ERK and Cbl protein-regulated signaling pathways, linking endogenous CDK16 to ERK phosphorylation and neurite outgrowth in neuroblastoma cells (Figure 6). Interestingly, we also observed increased phosphorylation of the closely related and even less studied family member CDK17 (Figure 5B and Table S3); thus, it could be speculated that this kinase exerts similar functions.

A conundrum of cell signaling is the concept of functional selectivity; how receptor-mediated activation of the same signaling pathways can lead to distinct cellular outcomes, as previously addressed with MS-based proteomics (Francavilla et al., 2013, 2016). Extensive studies in PC12 cells have shown that nerve growth factor (NGF) stimulation induces neurite outgrowth and differentiation, while epidermal growth factor (EGF) stimulation is associated with a strictly mitogenic response (Marshall, 1995; Traverse et al., 1992). These effects have been attributed to the differential NGF- and EGF-dependent signaling dynamics inducing sustained and transient ERK phosphorylation, respectively. The differential ERK signaling regulation and responses in PC12 cells have been explained by NGF mediating positive feedback loops from MAPK to Raf, whereas EGF only mediated negative feedback (Grewal et al., 1999; Kao et al., 2001; Santos et al., 2007). It has been shown that changes in phospho-ERK signaling at 24 hr of stimulation, but not at 5 min, had a predictive value for the neuronal differentiation and proliferation state at 48 hr, implying that sustained, but not short-term signals, ultimately determine cell fate outcomes (Chen et al., 2012). This illustrates the complex nature of ERK signaling and the importance of fine-tuned regulation for determination of cellular fate. Elucidating the exact molecular mechanisms mediating the sustained ERK phosphorylation response induced by Cbl protein depletion could likely depend on the development of other ways to manipulate Cbl function, in particular development of small-molecule inhibitors to target Cbl/Cbl-b. Our multi-level proteomics approach provides insights into how Cbl proteins regulate long-term global signaling responses related to sustained ERK phosphorylation and neurite outgrowth. We identify different proteins for which we functionally validate the role in the neurite outgrowth response induced by Cbl protein depletion. Thus, we hope our data can help to increase the understanding of the complex process of neuroblastoma cell differentiation and provide new avenues for further in-depth investigation.

Limitations of the study

The high level of heterogeneity characterizing neuroblastoma constitutes a challenge when studying this disease. Accordingly, observations such as those made in the present study might relate to subtypes of neuroblastoma tumors. Thus, while we do observe similar effects of Cbl and Cbl-b depletion in a panel of neuroblastoma cell lines, the magnitude of the effects differ between cell lines. This could potentially be due to intrinsic differences in protein expression and activity levels in the neuroblastoma cells and/or differential expression of known neuroblastoma oncogenes such as MYCN or ALK. For instance, ALK is amplified in the NB1 cells and known to drive their growth, which could explain the relatively high background level of ERK phosphorylation and the less obvious effect of Cbl/Cbl-b knockdown in these cells. However, this warrants further study. Differences in protein expression levels between cell lines can potentially also relate to different levels of dependency on Cbl proteins, which would result in varying effects of their depletion. Naturally, there is also an intrinsic limitation when using a model system based on siRNA-mediated depletion of target proteins as it is not possible to obtain complete protein ablation and there might be differences in transfection efficiency between cell lines. However, based on the need of this study to be performed with transient and simultaneous knockdown of Cbl and Cbl-b to induce a differentiation response, siRNA-based depletion was found to be the best approach. The need for approximately 24 h of siRNA treatment to yield sufficient knockdown levels constitutes another limitation in this type of study as compared to e.g. inhibitor-based studies. Accordingly, development of small-molecule inhibitors targeting Cbl/Cbl-b would enable characterization of short-term responses including changes in protein interaction partners and more immediate changes in global ubiquitylation and phosphorylation, which could aid interpretation of the long-term responses observed in the current manuscript.

Resource availability

Lead contact

Further information and requests for resources should be directed to and will be fulfilled by the lead contact, Dr. Jesper V. Olsen (jesper.olsen@cpr.ku.dk).

Materials availability

This study did not generate any new unique reagents.

Data and code availability

The accession number for the mass spectrometry proteomics data reported in this paper is [ProteomeX-change Consortium via PRIDE (Perez-Riverol et al., 2019)]: [PXD020389].

METHODS

All methods can be found in the accompanying [transparent methods supplemental file](#).

SUPPLEMENTAL INFORMATION

Supplemental information can be found online at <https://doi.org/10.1016/j.isci.2021.102321>.

ACKNOWLEDGMENTS

We thank members of the Proteomics Program at Novo Nordisk Foundation (NNF) Center for Protein Research (CPR) for valuable input and comments. Work at the Novo Nordisk Foundation Center for Protein Research (CPR) is funded in part by a generous donation from the Novo Nordisk Foundation (Grant number NNF14CC0001). We would like to thank the PRO-MS Danish National Mass Spectrometry Platform for Functional Proteomics and the CPR Mass Spectrometry Platform for instrument support and assistance, as well as the Protein Imaging Platform at CPR. A.P. was supported by the Novo Nordisk Foundation Copenhagen Bioscience PhD Programme grant (grant number NNF16CC0020906). C.F. was supported by a long-term EMBO fellowship (ALTF 746-2009) and the Wellcome Trust Sir Henry Dale fellowship 8107636/Z/15/Z. The work carried out in this study was supported by the Danish National Research Foundation (DNRF grant No. 141), Novo Nordisk Foundation (NNF18OC0052768), Danish Council for Technology and Production Sciences (DFF – 8022-00051), the European Union's 7th Framework Programme (Contract no. 259348-ASSET), and the European Union's Horizon 2020 research and innovation program under grant agreements: MSmed-686547, EPIC-XS-823839 and ERC synergy grant 810057-HighResCells.

AUTHOR CONTRIBUTIONS

A.K.P., D.B.B.J., V.A., and A.P. performed the experiments supervised by C.F. and J.V.O. G.K. developed automated image analysis software. A.K.P. and A.P. performed all downstream MS data analysis under supervision of J.V.O. V.A. and B.B. provided the protocol and supervision for ubiquitylome pulldown. A.K.P., A.P., C.F., and J.V.O. designed the experiments, critically evaluated the results, and wrote the manuscript. All authors read and approved the manuscript.

DECLARATION OF INTERESTS

The authors declare no competing interests.

Received: July 27, 2020

Revised: February 8, 2021

Accepted: March 15, 2021

Published: April 23, 2021

REFERENCES

- Akimov, V., Barrio-Hernandez, I., Hansen, S.V.F., Hallenborg, P., Pedersen, A.-K., Bekker-Jensen, D.B., Puglia, M., Christensen, S.D.K., Vanselow, J.T., Nielsen, M.M., et al. (2018). UbiSite approach for comprehensive mapping of lysine and N-terminal ubiquitination sites. *Nat. Struct. Mol. Biol.* 25, 631–640.
- Ambros, P.F., Ambros, I.M., Brodeur, G.M., Haber, M., Khan, J., Nakagawara, A., Schleiermacher, G., Speleman, F., Spitz, R., London, W.B., et al. (2009). International consensus for neuroblastoma molecular diagnostics: report from the International Neuroblastoma Risk Group (INRG) biology committee. *Br. J. Cancer* 100, 1471–1482.
- Axtman, A., Drewry, D., and Wells, C. (2019). N E W S & A N A L Y S I S Biobusiness Briefs CDK16 : the pick of the understudied PCTAIRE kinases. *Nat. Rev. Drug Discov.* 18, 489.
- Bekker-Jensen, D.B., Kelstrup, C.D., Batth, T.S., Larsen, S.C., Haldrup, C., Bramsen, J.B., Sørensen, K.D., Høyer, S., Ørntoft, T.F., Andersen, C.L., et al. (2017). An optimized shotgun strategy for the rapid generation of comprehensive human proteomes. *Cell Syst.* 4, 587–599.e4.
- Brodeur, G.M., and Bagatell, R. (2014). Mechanisms of neuroblastoma regression. *Nat. Rev. Clin. Oncol.* 11, 704–713.
- Chan, R.J., and Feng, G.-S. (2007). PTPN11 is the first identified proto-oncogene that encodes a tyrosine phosphatase. *Blood* 109, 862–867.
- Chen, B., Hammonds-odie, L., Perron, J., Masters, B.A., and Bixby, J.L. (2002). SHP-2 mediates target-regulated axonal termination and NGF-

- dependent neurite growth in sympathetic neurons *187*, 170–187.
- Chen, J.Y., Lin, J.R., Cimprich, K.A., and Meyer, T. (2012). A two-dimensional ERK-AKT signaling code for an NGF-triggered cell-fate decision. *Mol. Cell* *45*, 196–209.
- Chen, Y.N.P., Lamarche, M.J., Chan, H.M., Fekkes, P., Garcia-Foranet, J., Acker, M.G., Antonakos, B., Chen, C.H.T., Chen, Z., Cooke, V.G., et al. (2016). Allosteric inhibition of SHP2 phosphatase inhibits cancers driven by receptor tyrosine kinases. *Nature* *535*, 148–152.
- Cheung, N.-K.V., and Dyer, M.A. (2013). Neuroblastoma: developmental biology, cancer genomics and immunotherapy. *Nat. Rev. Cancer* *13*, 397–411.
- Chu, P.W.K., and Cheung, W.M.W. (2003). Differential effects of 9-cis, 13-cis and all-trans retinoic acids on the neuronal differentiation of human neuroblastoma cells *14*, 5–9.
- Cohn, S.L., Pearson, A.D.J., London, W.B., Monclair, T., Ambros, P.F., Brodeur, G.M., Faldut, A., Hero, B., Iehara, T., Machin, D., et al. (2009). The International Neuroblastoma Risk Group (INRG) classification system: an INRG task force report. *J. Clin. Oncol.* *27*, 289–297.
- Colaert, N., Helsens, K., Martens, L., Vandekerckhove, J., and Gevaert, K. (2009). Improved visualization of protein consensus sequences by iceLogo. *Nat. Methods* *6*, 786–787.
- Cooper, J.A., Kaneko, T., and Li, S.S.C. (2015). Cell regulation by phosphotyrosine-targeted ubiquitin ligases. *Mol. Cell Biol.* *35*, 1886–1897, MCB.00098–15.
- Dixon-Clarke, S.E., Shehata, S.N., Krojer, T., Sharpe, T.D., von Delft, F., Sakamoto, K., and Bullock, A.N. (2017). Structure and inhibitor specificity of the PCTAIRE-family kinase CDK16. *Biochem. J.* *474*, 699–713.
- Dohmen, M., Krieg, S., Agalaridis, G., Zhu, X., Shehata, S.N., Pfeifferberger, E., Amelang, J., Bütepage, M., Buerova, E., Pfaff, C.M., et al. (2020). AMPK-dependent activation of the Cyclin Y/CDK16 complex controls autophagy. *Nat. Commun.* *11*, 1–18.
- Edsjö, A., Holmquist, L., and Pahlman, S. (2007). Neuroblastoma as an experimental model for neuronal differentiation and hypoxia-induced tumor cell dedifferentiation. *Semin. Cancer Biol.* *17*, 248–256.
- Emdal, K.B., Pedersen, A.-K., Bekker-Jensen, D.B., Tsafou, K.P., Horn, H., Lindner, S., Schulte, J.H., Eggert, A., Jensen, L.J., Francavilla, C., et al. (2015). Temporal proteomics of NGF-TrkA signaling identifies an inhibitory role for the E3 ligase Cbl-b in neuroblastoma cell differentiation. *Sci. Signal.* *8*, ra40.
- Emdal, K.B., Pedersen, A.-K., Bekker-Jensen, D.B., Lundby, A., Claeys, S., De Preter, K., Speleman, F., Francavilla, C., and Olsen, J.V. (2018). Integrated proximal proteomics reveals IRS2 as a determinant of cell survival in ALK-driven neuroblastoma. *Sci. Signal.* *11*, 9752.
- Ettenberg, S.A., Magnifico, A., Cuello, M., Nau, M.M., Rubinstein, Y.R., Yarden, Y., Weissman, A.M., and Lipkowitz, S. (2001). Cbl-b-dependent coordinated degradation of the epidermal growth factor receptor signaling complex. *J. Biol. Chem.* *276*, 27677–27684.
- Francavilla, C., Rigbolt, K.T.G., Emdal, K.B., Carraro, G., Vernet, E., Bekker-Jensen, D.B., Streicher, W., Wikström, M., Sundström, M., Bellusci, S., et al. (2013). Functional proteomics defines the molecular switch underlying FGF receptor trafficking and cellular outputs. *Mol. Cell* *51*, 707–722.
- Francavilla, C., Papetti, M., Rigbolt, K.T.G., Pedersen, A.K., Sigurdsson, J.O., Cazzamali, G., Karemire, G., Blagoev, B., and Olsen, J.V. (2016). Multilayered proteomics reveals molecular switches dictating ligand-dependent EGFR trafficking. *Nat. Struct. Mol. Biol.* *23*, 608–618.
- Fredlund, E., Ringnér, M., Maris, J.M., and Pahlman, S. (2008). High Myc pathway activity and low stage of neuronal differentiation associate with poor outcome in neuroblastoma. *Proc. Natl. Acad. Sci. U S A* *105*, 14094–14099.
- Fu, W.Y., Cheng, K., Fu, A.K.Y., and Ip, N.Y. (2011). Cyclin-dependent kinase 5-dependent phosphorylation of Pctaire1 regulates dendrite development. *Neuroscience* *180*, 353–359.
- Graeser, R., Gannon, J., Poon, R.Y.C., Dubois, T., Aitken, A., and Hunt, T. (2002). Regulation of the CDK-related protein kinase PCTAIRE-1 and its possible role in neurite outgrowth in Neuro-2A cells. *J. Cell Sci.* *115*, 3479–3490.
- Grewal, S.S., York, R.D., and Stork, P.J.S. (1999). Extracellular-signal-regulated kinase signalling in neurons. *Curr. Opin. Neurobiol.* *9*, 544–553.
- Guerreiro, A.S., Boller, D., Shalaby, T., Grotzer, M.A., and Arcaro, A. (2006). Protein kinase B modulates the sensitivity of human neuroblastoma cells to insulin-like growth factor receptor inhibition. *Int. J. Cancer* *119*, 2527–2538.
- Halder, D., Kim, G.-H., and Shin, I. (2015). Synthetic small molecules that induce neuronal differentiation in neuroblastoma and fibroblast cells. *Mol. Biosyst.* *11*, 2727–2737.
- Hanafusa, H., Torii, S., Yasunaga, T., Matsumoto, K., and Nishida, E. (2004). Shp2, an SH2-containing protein-tyrosine phosphatase, positively regulates receptor tyrosine kinase signaling by dephosphorylating and inactivating the inhibitor sprouty. *J. Biol. Chem.* *279*, 22992–22995.
- Irwin, M.S., and Park, J.R. (2015). Neuroblastoma paradigm for precision medicine. *Pediatr. Clin. North Am.* *62*, 225–256.
- Jafari, R., Almqvist, H., Axelsson, H., Ignatushchenko, M., Lundbäck, T., Nordlund, P., and Molina, D.M. (2014). The cellular thermal shift assay for evaluating drug target interactions in cells. *Nat. Protoc.* *9*, 2100–2122.
- Johnsen, J.I., Dyberg, C., Fransson, S., and Wickström, M. (2018). Molecular mechanisms and therapeutic targets in neuroblastoma. *Pharmacol. Res.* *131*, 164–176.
- Kao, S.C., Jaiswal, R.K., Kolch, W., and Landreth, G.E. (2001). Identification of the mechanisms regulating the differential activation of the MAPK cascade by epidermal growth factor and nerve growth factor in PC12 cells. *J. Biol. Chem.* *276*, 18169–18177.
- Kim, B., Leventhal, P.S., Saltiel, A.R., and Feldman, E.L. (1997). Insulin-like growth factor-I-mediated neurite outgrowth in vitro requires mitogen-activated protein kinase activation. *J. Biol. Chem.* *272*, 21268–21273.
- Lavenius, E., Parrow, V., Nånberg, E., and Pahlman, S. (1994). Basic FGF and IGF-I promote differentiation of human SH-SY5y neuroblastoma cells in culture. *Growth Factors* *10*, 29–39.
- Li, H., Xu, L., Li, C., Zhao, L., Ma, Y., Zheng, H., Li, Z., Zhang, Y., Wang, R., Liu, Y., et al. (2014). Ubiquitin ligase Cbl-b represses IGF-I-induced epithelial mesenchymal transition via ZEB2 and microRNA-200c regulation in gastric cancer cells. *Mol. Cancer* *13*, 136.
- Malumbres, M. (2014). Cyclin-dependent kinases. *Genome Biol.* *15*, 122.
- Marshall, C.J. (1995). Specificity of receptor tyrosine kinase signaling: transient versus sustained extracellular signal-regulated kinase activation. *Cell* *80*, 179–185.
- Matthay, K.K., Reynolds, C.P., Seeger, R.C., Shimada, H., Adkins, E.S., Haas-Kogan, D., Gerbing, R.B., London, W.B., and Villablanca, J.G. (2009). Long-term results for children with high-risk neuroblastoma treated on a randomized trial of myeloablative therapy followed by 13-cis-retinoic acid: a children's oncology group study. *J. Clin. Oncol.* *27*, 1007–1013.
- Matthay, K.K., Maris, J.M., Schleiermacher, G., Nakagawara, A., Mackall, C.L., Diller, L., and Weiss, W.A. (2016). Neuroblastoma. *Nat. Rev. Dis. Primers* *2*, 16078.
- Mazot, P., Cazes, A., Dingli, F., Degoutin, J., Irinopoulou, T., Bouterin, M.C., Lombard, B., Loew, D., Hallberg, B., Palmer, R.H., et al. (2012). Internalization and down-regulation of the ALK receptor in neuroblastoma cell lines upon monoclonal antibodies treatment. *PLoS One* *7*, 1–10.
- Miyake, S., Lupper, M.L., Druker, B., and Band, H. (1998). The tyrosine kinase regulator Cbl enhances the ubiquitination and degradation of the platelet-derived growth factor receptor alpha. *Proc. Natl. Acad. Sci. U S A* *95*, 7927–7932.
- Mohapatra, B., Ahmad, G., Nadeau, S., Zutshi, N., An, W., Scheffe, S., Dong, L., Feng, D., Goetz, B., Arya, P., et al. (2013). Protein tyrosine kinase regulation by ubiquitination: critical roles of Cbl-family ubiquitin ligases. *Biochim. Biophys. Acta* *1833*, 122–139.
- Mohlin, S.A., Wigerup, C., and Pahlman, S. (2011). Neuroblastoma aggressiveness in relation to sympathetic neuronal differentiation stage. *Semin. Cancer Biol.* *21*, 276–282.
- Mokalled, M.H., Johnson, A., Kim, Y., Oh, J., and Olson, E.N. (2010). Myocardin-related transcription factors regulate the Cdk5/Pctaire1 kinase cascade to control neurite outgrowth, neuronal migration and brain development. *Development* *137*, 2365–2374.
- Motegi, A., Fujimoto, J., Kotani, M., Sakuraba, H., and Yamamoto, T. (2004). ALK receptor tyrosine

kinase promotes cell growth and neurite outgrowth. *J. Cell Sci.* 117, 3319–3329.

Nishimura, N., Goji, J., Nakamura, H., Orita, S., Takai, Y., and Sano, K. (1995). Cloning of a brain-type isoform of human Rab GDI and its expression in human neuroblastoma cell lines and tumor specimens. *Cancer Res.* 55, 5445–5450.

Påhlman, S., Hoehner, J.C., Nånberg, E., Hedborg, F., Fagerström, S., Gestblom, C., Johansson, I., Larsson, U., Lavenius, E., Örtoft, E., et al. (1995). Differentiation and survival influences of growth factors in human neuroblastoma. *Eur. J. Cancer* 31, 453–458.

Perez-Riverol, Y., Zorin, A., Dass, G., Vu, M.-T., Xu, P., Glont, M., Vizcaino, J.A., Jarnuczak, A.F., Petryszak, R., Ping, P., et al. (2019). Quantifying the impact of public omics data. *Nat. Commun.* 10 (3512).

Perrinjaquet, M., and Iba, C.F. (2010). Protein-tyrosine phosphatase SHP2 contributes to GDNF neurotrophic activity through direct binding to phospho-tyr 687 in the RET receptor tyrosine kinase * 285, 31867–31875.

Petrelli, A., Gilestro, G.F., Lanzardo, S., Comoglio, P.M., Migone, N., and Giordano, S. (2002). The endophilin-CIN85-Cbl complex mediates ligand-dependent downregulation of c-Met. *Nature* 416, 187–190.

Påhlman, S., Ruusala, A.I., Abrahamsson, L., Mattsson, M.E.K., and Esscher, T. (1984). Retinoic acid-induced differentiation of cultured human neuroblastoma cells: a comparison with phorbol-ester-induced differentiation. *Cell Differ.* 14, 135–144.

Ratner, N., Brodeur, G.M., Dale, R.C., and Schor, N.F. (2016). The “neuro” of neuroblastoma: neuroblastoma as a neurodevelopmental disorder. *Ann. Neurol.* 80, 13–23.

Reckel, S., Hamelin, R., Georgeon, S., Armand, F., Jolliet, Q., Chiappe, D., Moniatte, M., and Hantschel, O. (2017). Differential signaling networks of Bcr-Abl p210 and p190 kinases in leukemia cells defined by functional proteomics. *Leukemia* 31, 1502–1512.

Rettig, I., Koeneke, E., Trippel, F., Mueller, W.C., Burhenne, J., Kopp-Schneider, A., Fabian, J.,

Schober, A., Ferekorn, U., von Deimling, A., et al. (2015). Selective inhibition of HDAC8 decreases neuroblastoma growth in vitro and in vivo and enhances retinoic acid-mediated differentiation. *Cell Death Dis.* 6, e1657.

Robinson, M.J., Stippec, S.A., Goldsmith, E., White, M.A., and Cobb, M.H. (1998). A constitutively active and nuclear form of the MAP kinase ERK2 is sufficient for neurite outgrowth and cell transformation. *Curr. Biol.* 8, 1141–1150.

Rorsman, C., Tsioumpkou, M., Heldin, C.-H., and Lennartsson, J. (2016). The ubiquitin ligases c-Cbl and Cbl-b negatively regulate PDGF-BB-induced chemotaxis by affecting PDGFRβ internalization and signaling. *J. Biol. Chem.* 291, 11608–11618.

Santos, S.D.M., Verveer, P.J., and Bastiaens, P.I.H. (2007). Growth factor-induced MAPK network topology shapes Erk response determining PC-12 cell fate. *Nat. Cell Biol.* 9, 324–330.

Sehat, B., Andersson, S., Girnita, L., and Larsson, O. (2008). Identification of c-Cbl as a new ligase for insulin-like growth factor-I receptor with distinct roles from Mdm2 in receptor ubiquitination and endocytosis. *Cancer Res.* 68, 5669–5677.

Shtiegman, K., Kochupurakkal, B.S., Zwang, Y., Pines, G., Starr, A., Vexler, A., Citri, A., Katz, M., Lavi, S., Ben-Basat, Y., et al. (2007). Defective ubiquitination of EGFR mutants of lung cancer confers prolonged signaling. *Oncogene* 26, 6968–6978.

Soubeyran, P., Kowanetz, K., Szymkiewicz, I., Langdon, W.Y., and Dikic, I. (2002). Cbl-CIN85-endophilin complex mediates ligand-induced downregulation of EGF receptors. *Nature* 416, 183–187.

Takahashi, Y., Shimokawa, N., Esmaeili-Mahani, S., Morita, A., Masuda, H., Iwasaki, T., Tamura, J., Ichi, Haglund, K., and Koibuchi, N. (2011). Ligand-induced downregulation of TrkA is partly regulated through ubiquitination by Cbl. *FEBS Lett.* 585, 1741–1747.

Tanno, B., Mancini, C., Vitali, R., Mancuso, M., McDowell, H.P., Dominici, C., and Raschella, G. (2006). Down-regulation of insulin-like growth factor I receptor activity by NVP-AEW541 has an

antitumor effect on neuroblastoma cells in vitro and in vivo. *Clin. Cancer Res.* 12, 6772–6780.

Thien, C.B., and Langdon, W.Y. (2001). Cbl: many adaptations to regulate protein tyrosine kinases. *Nat. Rev. Mol. Cell Biol.* 2, 294–307.

Traverse, S., Gomez, N., Paterson, H., Marshall, C., and Cohen, P. (1992). Sustained activation of the mitogen-activated protein (MAP) kinase cascade may be required for differentiation of PC12 cells. *Biochem. J.* 288, 351–355.

Van den Eynden, J., Umopathy, G., Ashouri, A., Cervantes-Madrid, D., Szydzik, J., Ruuth, K., Koster, J., Larsson, E., Guan, J., and Palmer, R.H. (2018). Phosphoproteome and gene expression profiling of ALK inhibition in neuroblastoma cell lines reveals conserved oncogenic pathways. *Sci. Signal.* 11.

Veal, G.J., Errington, J., Redfern, C.P.F., Pearson, A.D.J., and Boddy, A.V. (2002). Influence of isomerisation on the growth inhibitory effects and cellular activity of 13-cis and all-trans retinoic acid in neuroblastoma cells. *Biochem. Pharmacol.* 63, 207–215.

Wong, A., Lamothe, B., Lee, A., Schlessinger, J., Lax, I., and Li, A. (2002). FRS2 alpha attenuates FGF receptor signaling by Grb2-mediated recruitment of the ubiquitin ligase Cbl. *Proc. Natl. Acad. Sci. U S A* 99, 6684–6689.

Wright, J.H., Druceckes, P., Bartoe, J., Zhao, Z., Shen, S.-H., and Krebs, E.G. (1997). A role for the SHP-2 tyrosine phosphatase in nerve growth factor-induced PC12 cell differentiation 8, 1575–1585.

Yokouchi, M., Wakioka, T., Sakamoto, H., Yasukawa, H., Ohtsuka, S., Sasaki, A., Ohtsubo, M., Valius, M., Inoue, A., Komiya, S., et al. (1999). APS, an adaptor protein containing PH and SH2 domains, is associated with the PDGF receptor and c-Cbl and inhibits PDGF-induced mitogenesis. *Oncogene* 18, 759–767.

Zhao, Q., Tran, H., Dimitrov, D.S., and Cheung, N.K.V. (2015). A dual-specific anti-IGF-1/IGF-2 human monoclonal antibody alone and in combination with temsirolimus for therapy of neuroblastoma. *Int. J. Cancer* 137, 2243–2252.

iScience, Volume 24

Supplemental information

Proteomic investigation of Cbl and Cbl-b

in neuroblastoma cell differentiation

highlights roles for SHP-2 and CDK16

Anna-Kathrine Pedersen, Anamarija Pfeiffer, Gopal Karemore, Vyacheslav Akimov, Dorte B. Bekker-Jensen, Blagoy Blagoev, Chiara Francavilla, and Jesper V. Olsen

A

Cell line	MYCN status	ALK status
SH-SY5Y	Single copy	F1174L
NB1	Amplification	Amplification
IMR-32	Amplification	WT

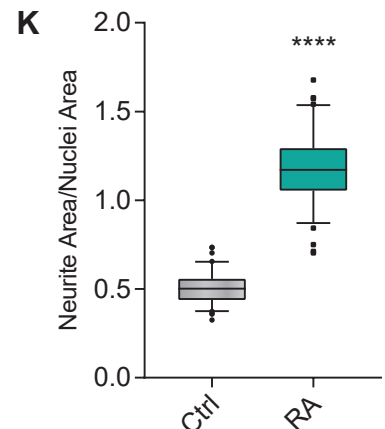
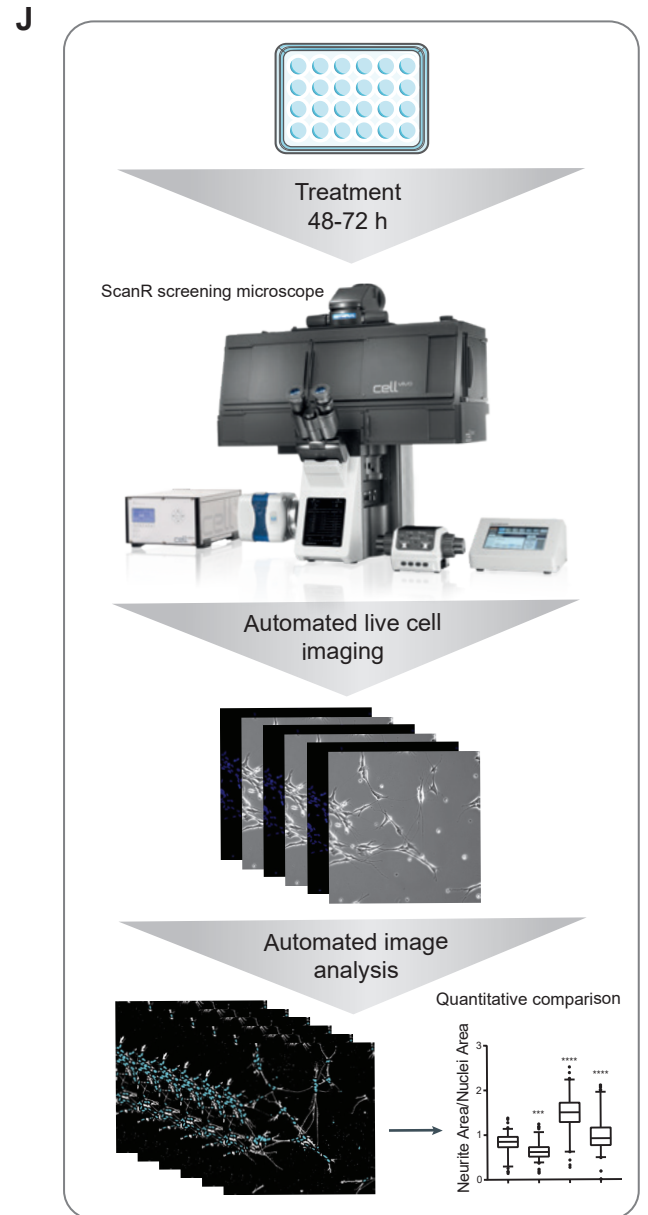
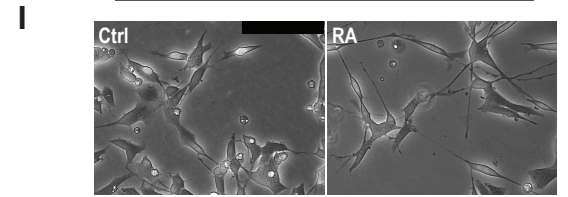
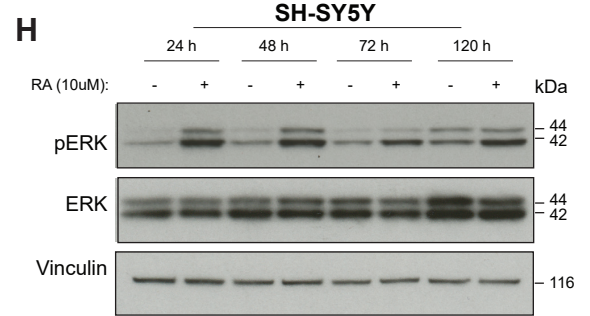
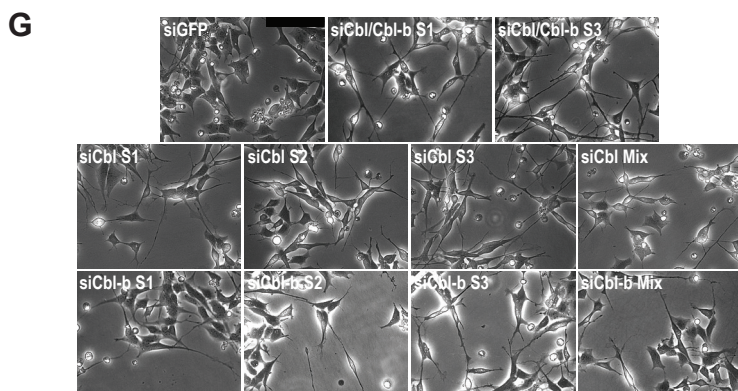
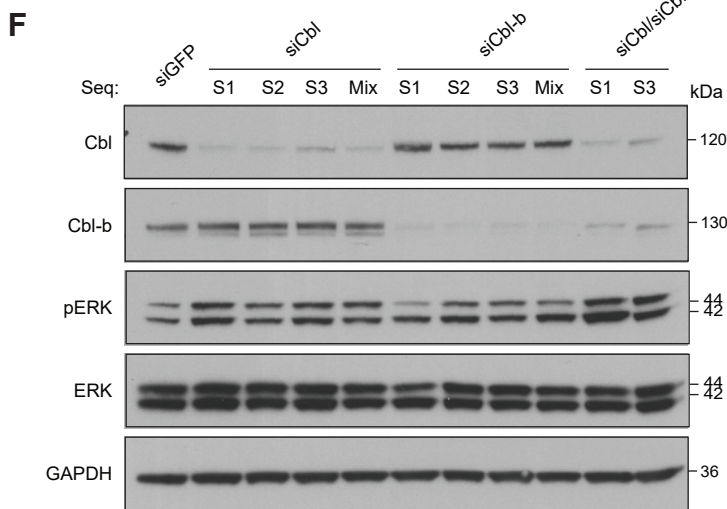
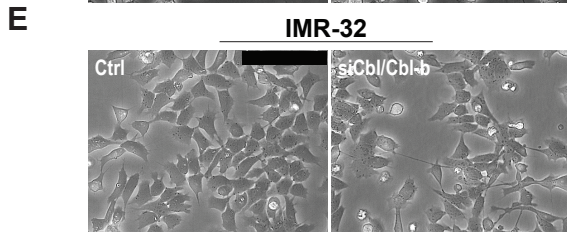
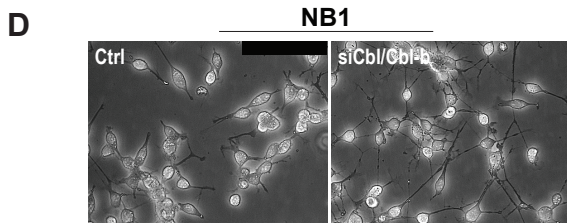
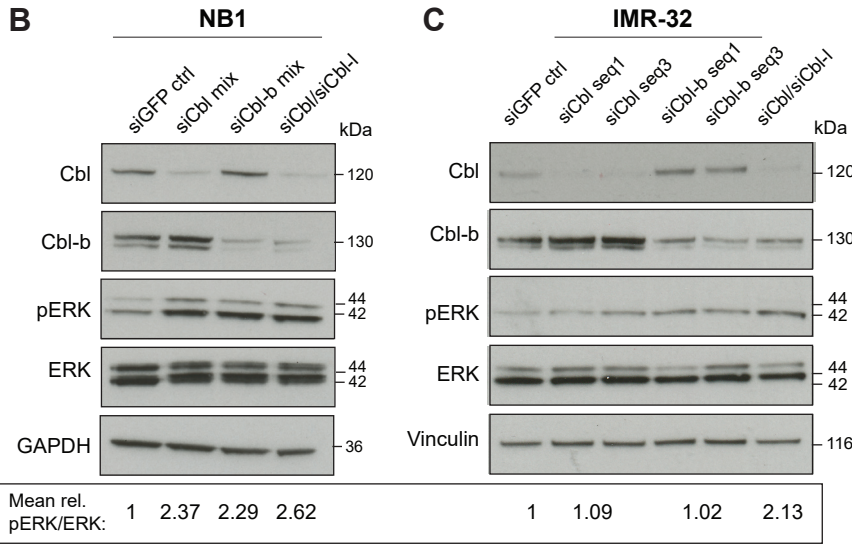


Figure S1. Depletion of Cbl/Cbl-b and RA stimulation leads to increased ERK phosphorylation levels associated with increased neurite outgrowth in neuroblastoma cell lines, Related to Figure 1. (A) Table of the three applied neuroblastoma cell lines. **(B-C)** Lysates from NB1 **(B)** or IMR-32 **(C)** cells treated with control siRNA or siRNA against Cbl and/or Cbl-b for 48-72 hours, were immunoblotted detecting the indicated proteins and quantified as shown below. Data are representative of two independent experiments (n=2). **(D-E)** Representative images showing visualization of neurite outgrowth of NB1 and IMR32 cells, respectively, treated with Ctrl or Cbl/Cbl-b siRNA, (scale bar, 50 μ m). **(F-G)** SH-SY5Y cells were treated with siRNA against Cbl and/or Cbl-b (as indicated) for 72 hours. **(F)** Lysates were subjected to immunoblotting with antibodies against phospho-ERK/ERK or Cbl/Cbl-b. **(G)** Representative images for neurite outgrowth visualization (same conditions as in F). Data are representative of three independent experiments (n=3) **(H)** Lysates from SH-SY5Y cells treated with 10 μ M RA for 24 to 120 hours, were immunoblotted detecting the indicated proteins. **(I)** Representative images for visualization of neurite outgrowth of SH-SY5Y cells after 72 hours of RA treatment. **(J)** Workflow illustrating automated neurite outgrowth analysis. **(K)** Quantification of neurite outgrowth of SH-SY5Y cells after 72 h of treatment with RA or DMSO. Data are shown as medians w. 95% CI and representative of two independent experiments (n=2). **** indicates $P < 0.0001$ (t-test).

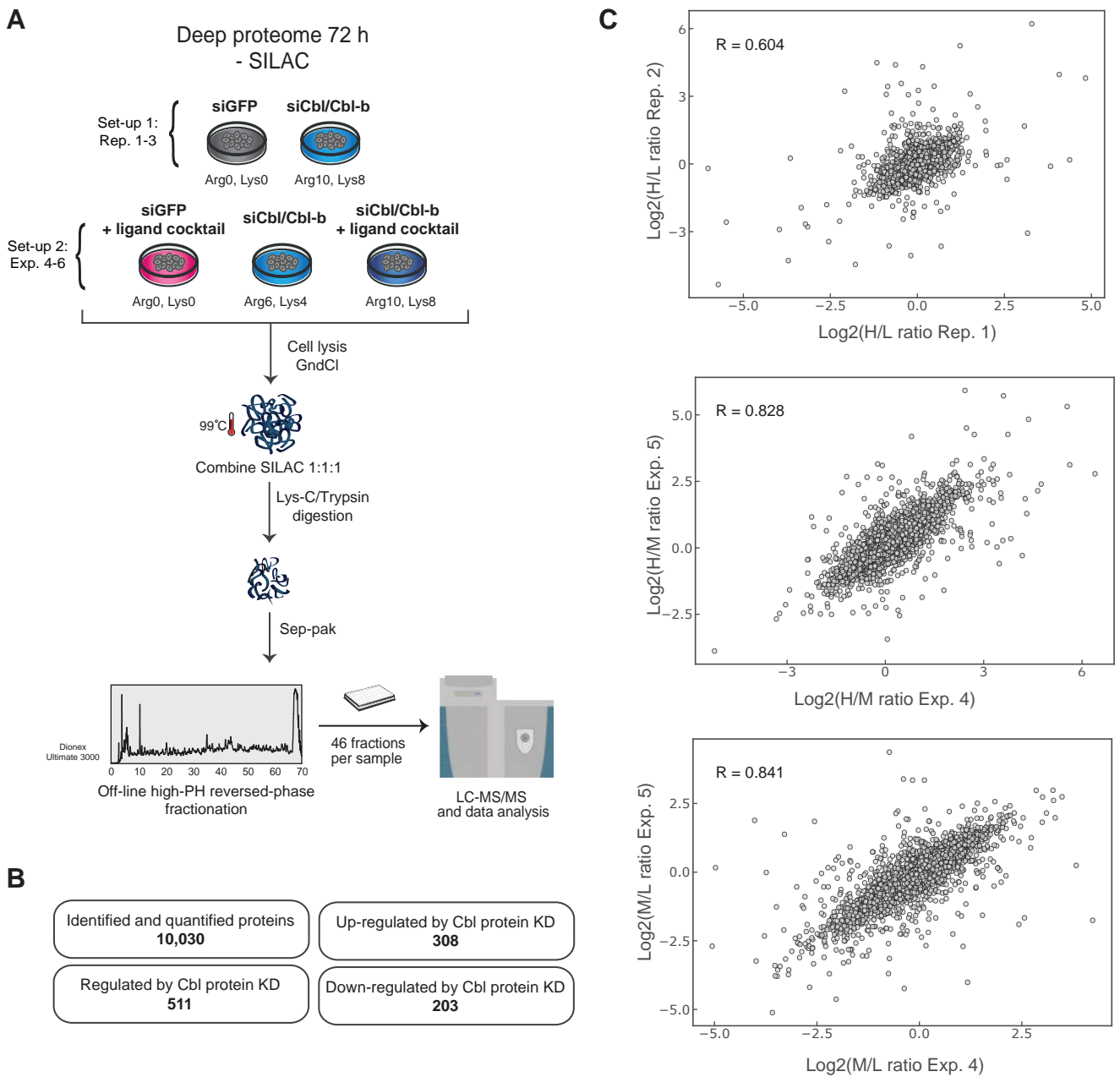


Figure S2. Deep proteome analysis of SH-SY5Y cells shows good quality controls, Related to Figure 2 and Table S1. (A) Experimental design and workflow of SILAC-based deep proteome analysis of Cbl and Cbl-b dependent long-term signaling in SH-SY5Y cells. Cells were treated with control or Cbl/Cbl-b siRNA combined with stimulation with RTK ligand cocktail (FGF-2, IGF-1, PDGF-BB, TGF α) for a total of 72 hours as indicated. (B) Overview of proteome data showing the numbers of identified proteins and proteins regulated by Cbl protein knockdown (as presented in Fig. 2D). (C) Representative correlation plots of normalized SILAC protein ratios between biological replicates with R indicating Pearson correlation coefficients.

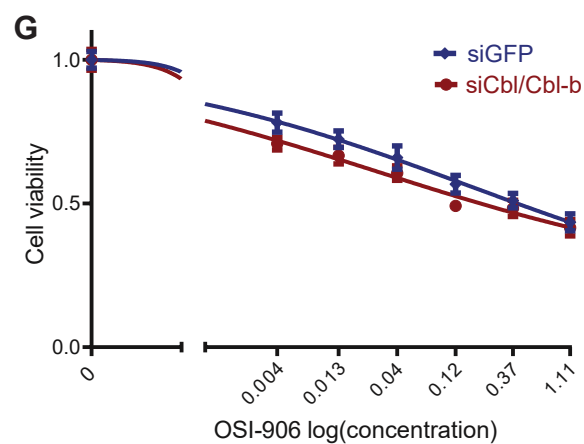
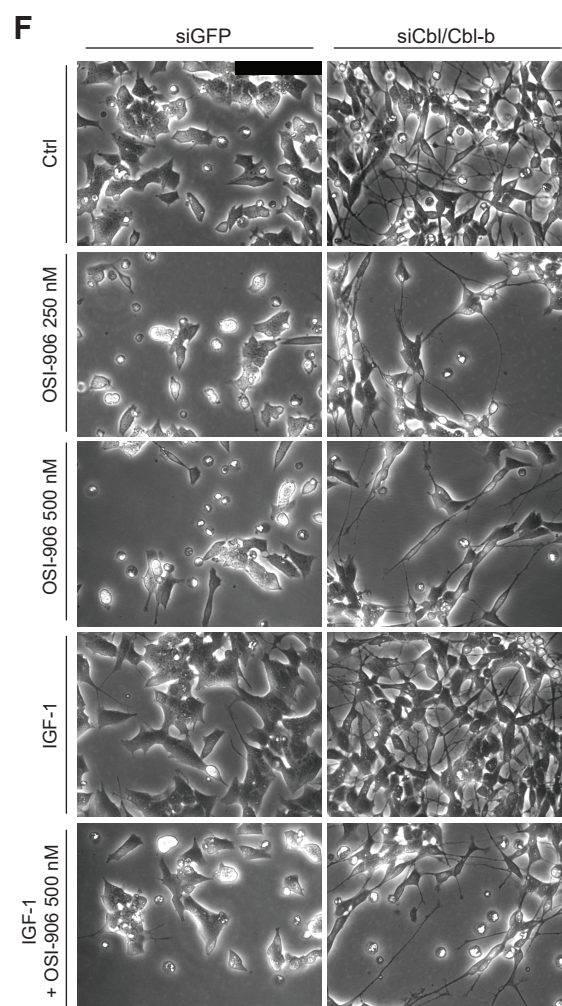
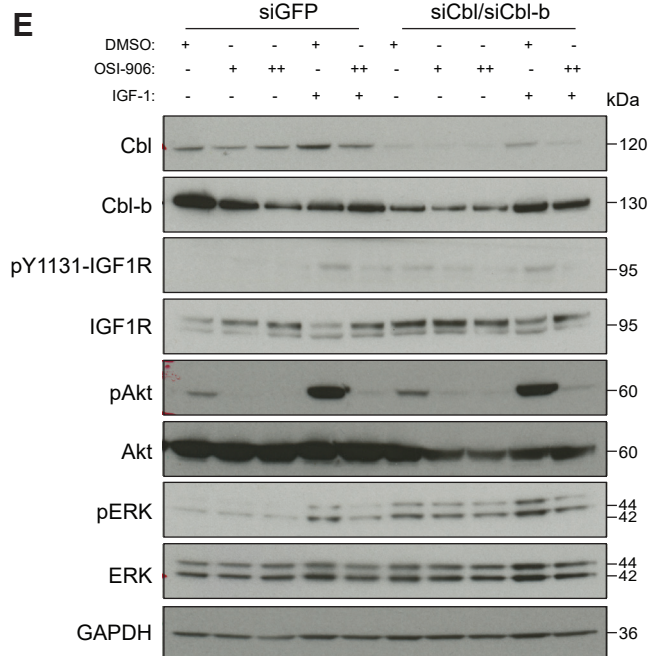
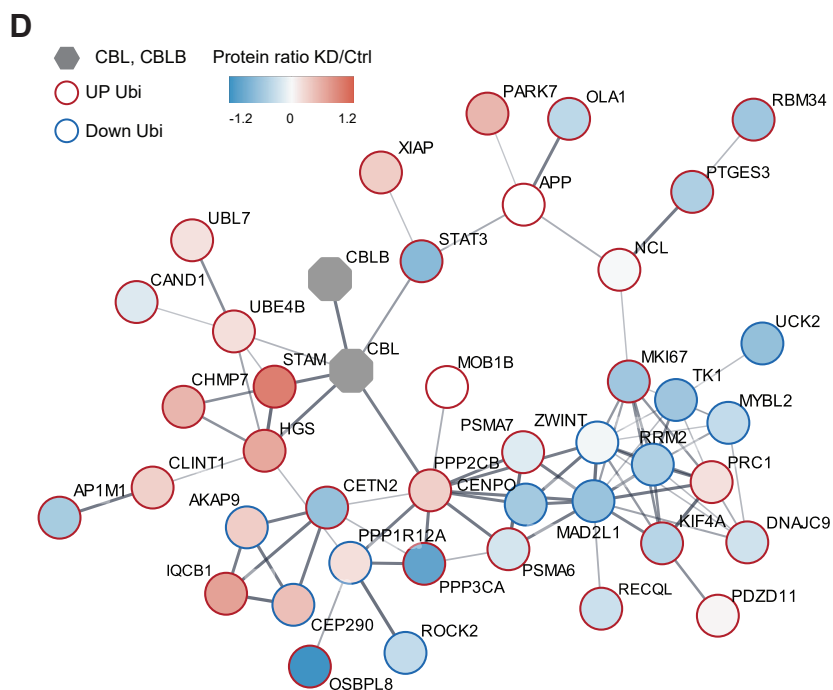
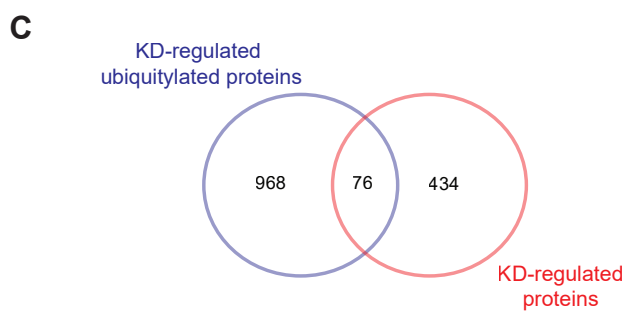
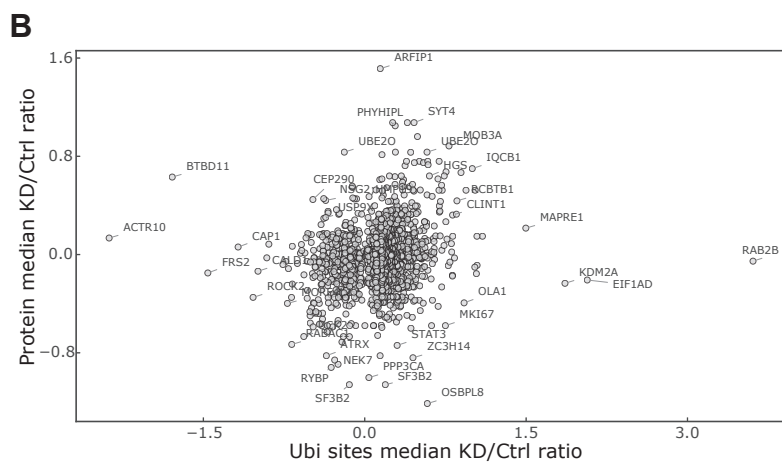
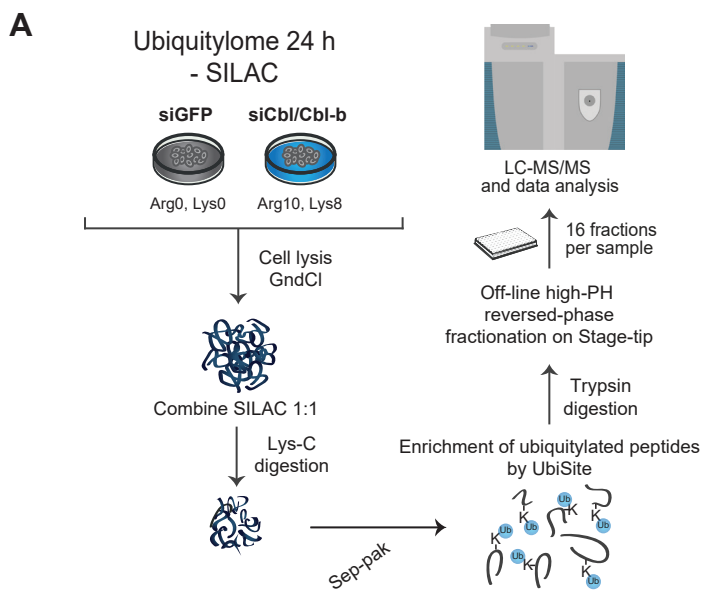


Figure S3. The ubiquitylome of Cbl/Cbl-b-depleted SH-SY5Y cells and the role of IGF1R activity in Cbl/Cbl-b-mediated control of ERK phosphorylation and neurite outgrowth, Related to Figure 3 and Table S1 and S2. (A) Experimental workflow for ubiquitylome analysis of SH-SY5Y cells depleted of Cbl and Cbl-b. **(B)** Correlation between ratios of regulated ubiquitin sites and the ratio of their corresponding protein as identified in the 72 hour-proteome data. Selected gene names are indicated. **(C)** Venn diagram showing the overlap between proteins with regulated ubiquitylation sites and proteins regulated at 72 hours by siCbl/Cbl-b treatment. **(D)** Cbl/Cbl-b connected network as identified by functional network analysis of the 76 shared regulated proteins found in (C). Node color indicates regulation at protein level and outer circle indicates regulation of ubiquitin sites (blue: Down, red: Up). **(E)** Immunoblotting of lysates from SH-SY5Y cells treated with siGFP or siCbl/Cbl-b and IGF1R inhibitor (Linsitinib/OSI-906; + and ++ indicates 250 or 500 nM, respectively) for 72 hours, using the indicated antibodies. **(F)** Representative images based on the same conditions as in (E), (scale bar, 50 μ m). Data are representative of three independent experiments (n=3). **(G)** Cell viability of SH-SY5Y siCbl/Cbl-b or siGFP-treated cells in response to increasing doses of OSI-906 for 72 h. Data is presented as means \pm SEM, (n=3).

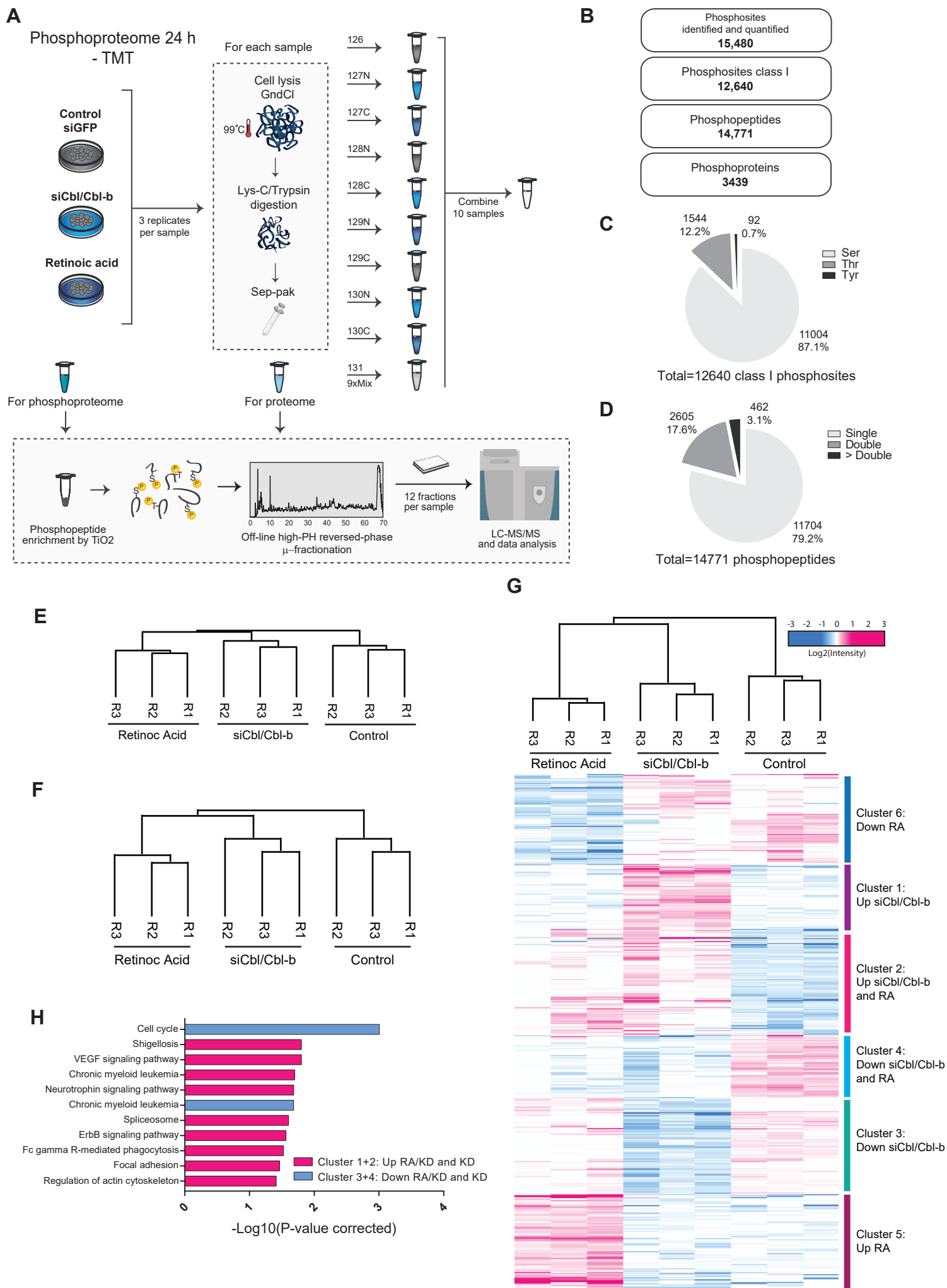


Figure S4. Overview of 24-hour phosphoproteome and proteome analysis of Cbl/Cbl-b depleted and RA stimulated SH-SY5Y cells, Related to Figure 4 and Table S3 and S4. (A) Experimental workflow for TMT10plex-based phosphoproteome and proteome analysis of SH-SY5Y cells depleted for Cbl and Cbl-b or treated with RA for 24 hours. **(B)** Overview of phosphoproteomics data. **(C)** Distribution of identified class I phosphorylation sites by amino acid. **(D)** Distribution of identified phosphopeptides with one, two or more than two phosphorylated sites. **(E-F)** Quality control of phosphoproteome data **(E)** and proteome data **(F)** by unsupervised hierarchical clustering using normalized intensities for identified and quantified phosphorylation sites or proteins, respectively. **(G)** Hierarchical clustering of proteins with significantly regulated abundance (ANOVA) in response to treatment with Cbl/Cbl-b siRNA or RA for 24 hours. The six identified clusters selected for further analyses are highlighted on the right. Data are presented with log₂ normalized TMT intensities. **(H)** Bar graph showing results of KEGG pathway enrichment analysis for phospho clusters 1+2 (pink) and 3+4 (blue).

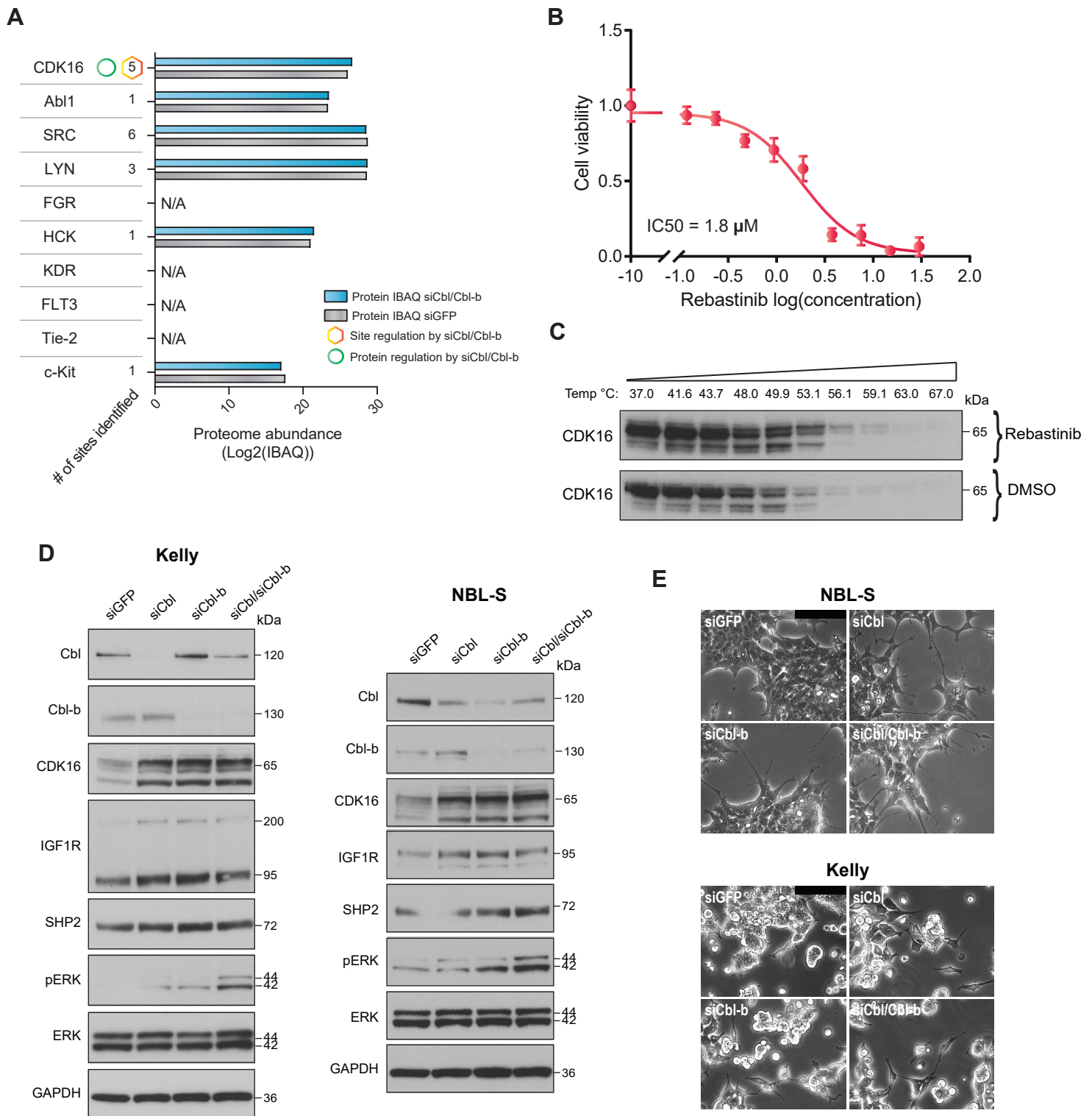


Figure S5. Rebastinib targets CDK16 in SH-SY5Y cells, Related to Figure 5. (A) Bar graph showing protein abundance (Log₂(IBAQ) values) of Rebastinib off-targets and CDK16. N/A: Not available. The number of identified phosphorylation sites for each protein is indicated and circles indicate if a site or protein was identified as regulated by Cbl/Cbl-b knockdown. **(B)** Cell viability of SH-SY5Y cells in response to treatment with different concentrations of Rebastinib for 48 h for IC₅₀ determination (IC₅₀=1.8 μM). Data is presented as means ± SEM of 4 replicates. **(C)** For cellular thermal shift assay aliquots of Rebastinib- or DMSO-treated cells were heated at the indicated temperatures and subjected to immunoblotting with antibody against CDK16. **(D-E)** Kelly and NBL-S cells were treated with siRNA against Cbl and/or Cbl-b (as indicated) for 72 hours. **(D)** Lysates were subjected to immunoblotting with antibodies against the indicated proteins. **(E)** Representative images for neurite outgrowth visualization (same conditions as in D), (scale bar, 50 μm). Data is representative of three independent experiments (n=3).

Transparent Methods

Cell Culture and SILAC Labeling

The human neuroblastoma cell lines SH-SY5Y, NB1, NBL-S, Kelly and IMR-32 were cultured in RPMI 1640 with 2 mM L-glutamine (Gibco) supplemented with 10% fetal bovine serum (Gibco) and penicillin-streptomycin (100 U/mL and 100 µg/ml, Gibco). Cells were maintained at 37°C in a humidified incubator with 5% CO₂. All cell lines were tested negative for mycoplasma. For stable isotope labeling by amino acids in cell culture (SILAC)-based quantitative mass spectrometry, SH-SY5Y cells were grown and labeled for a minimum of two weeks in SILAC RPMI (PAA Laboratories), to yield three differentially labeled cell populations: Light Arg0/Lys0 (labeled with natural variants of Arginine and Lysine), medium Arg6/Lys4 (labeled with medium variants of the amino acids L-[13C6]Arg (+6) and L-[2H4]Lys (+4) and heavy Arg10/Lys8 (labeled with heavy variants of the amino acids L-[13C6,15N4]Arg (+10) and L-[13C6,15N2]Lys (+8)). No label swap was done for SILAC experiments. Light amino acids were purchased from Sigma and medium and heavy amino acids were from Cambridge isotope Labs. SILAC RPMI was supplemented with 10% dialyzed fetal bovine serum (Gibco), 2 mM L-glutamine (Gibco) and penicillin-streptomycin (100 U/mL and 100 µg/ml, Gibco).

Experimental treatment/stimulation of cell cultures

Cells were cultured in complete medium and starved in serum-free medium for 6 hours before short-term stimulation (10-120 min) with ligands (20-100 ng/ml of FGF-2, IGF-1, PDGF-BB or TGFα (Peprotech)) either individually or in a mixture (referred to as “ligand cocktail”). For long-term stimulation (24-72 hours) cells were kept in 0.5% FBS medium and ligands were replenished every 24 hours. For retinoic acid (RA, Sigma-Aldrich) treatment, cells were incubated with 10 µM RA (in complete medium) for indicated time points. For experiments including chemical inhibition, cells were treated for 48-72 hours with the indicated concentration of inhibitor (U0126 (Cell Signaling Technology), OSI-906, NVP-AEW541, SHP099 or Rebastinib (Selleckchem)). The control condition was treated with a final concentration 0.1% DMSO (Sigma-Aldrich) corresponding to amounts for RA- or inhibitor-treated cells (siRNA transfection of cell cultures is described separately below).

Transfection and RNA Interference

For siRNA-mediated knockdown, SH-SY5Y, NB1 and IMR-32 were transfected with target or control siRNA using Lipofectamine RNAiMAX with OptiMem (both Thermo Fisher Scientific/Invitrogen) according to the instructions of the manufacturer. Double-stranded siRNA oligonucleotides targeting human CBL:

(sequence #1: 5'-CCAGCAGAUUGAUAGCUGUACGUAAU-3';

sequence #2: 5'-GCGGAGAAUCAACUCUGAACGGAAA-3';

sequence #3: 5'-CCUACCAGGACAUCAGAAAGCUUU-3')

and targeting CBLB:

(sequence #1: 5'-UCAUCCCACCCUGUUUCCCUGAAUU-3';

sequence #2: 5'-GGUCCAUCUUCAGAGAAGAAAUCAA-3';

sequence #3: 5'-CAUGGGAGAGGGUUAUGCCUUUGAA-3')

and targeting CDK16:

(sequence: 5'-ACAUCGUUACGCUACAUGAtt-3')

were acquired from (Thermo Fisher Scientific/Invitrogen). For single protein knockdown, cells were transfected with either individual or mixtures of siRNA sequences (as indicated) and for simultaneous knockdown of both Cbl and Cbl-b, cells were transfected with the targeting sequences #3. Experiments were performed with a final siRNA concentration of 25 nM or 50 nM for CDK16 knockdown, and all assays were carried out 24-72 hours post transfection. As a negative control, cells were transfected with Stealth RNAi siRNA GFP Reporter Control duplex (Thermo Fisher Scientific/Invitrogen) in a final concentration corresponding to target siRNAs (25 nM). The knockdown efficiency of target genes was assessed by Western blotting of cell lysates with specific antibodies against Cbl and Cbl-b or CDK16.

Cell lysis, SDS-PAGE and western blotting

For western blotting, cells were washed with phosphate-buffered saline (PBS) and lysed in radio-immunoprecipitation assay (RIPA) buffer (50 mM Tris-HCl pH7.5, 150 mM NaCl, 1 mM EDTA, 1% NP-40, 0.1% sodium deoxycholate with the addition of 5 mM β -glycerophosphate, 5 mM sodium fluoride, 1 mM sodium orthovanadate and 1 cOmplete Protease Inhibitor Cocktail tablet (Roche/Merck) pr. 10 mL of lysis buffer. Protein concentrations were quantified using the Pierce BCA Protein Assay Kit (ThermoFisher Scientific). Proteins were separated by SDS-PAGE using NuPAGE 4-12% Bis-Tris Protein Gels (Invitrogen/Thermo Fisher Scientific) under denaturing and reducing conditions with MOPS SDS running buffer (Invitrogen/Thermo Fisher Scientific) and transferred onto nitrocellulose membranes (Sigma-Aldrich). Membranes were blocked in phosphate-buffered saline (PBS) and 0.1% Tween-20 with either 5% bovine serum albumin (BSA) (Sigma-Aldrich) or 5% skim milk powder (Sigma-Aldrich), before incubation with primary antibody overnight at 4°C. Membranes were incubated for 1 hour with species-specific horseradish peroxidase (HRP)-conjugated secondary antibody and developed and visualized using Novex ECL Chemiluminescent Substrate Reagent Kit (Invitrogen/Thermo Fisher Scientific) and Amersham Hyperfilm (GE Healthcare). For the detection of multiple proteins on the same membrane, antibodies were removed using a stripping buffer [500 mM glycine, pH2.5] and reprobbed with a new primary antibody. The ImageJ software was used to quantify the intensity of the protein bands.

The following antibodies were used in this study: rabbit anti-phospho-Akt (Ser473), rabbit anti-Akt, mouse anti-phospho-ERK1/2 (Thr202/Tyr204), rabbit anti-ERK1/2, rabbit anti-PDGFR β , rabbit anti-Shp-2, rabbit anti-phospho-IGFR1/INSR (Tyr1131/Tyr1146), rabbit anti-IGF1R, anti rabbit-PCTaire1/CDK16 (Cell Signaling Technology), rabbit anti-Cbl, rabbit anti-Cbl-b (Santa Cruz Biotechnology), rabbit anti-EGFR (Millipore), mouse anti-GAPDH (abcam), mouse anti-Vinculin (Sigma-Aldrich), goat-anti-mouse and goat-anti-rabbit HRP-conjugated secondary antibody (Jackson ImmunoResearch Laboratories).

Cell viability assay – IC50 determination

Cells were seeded in 96-well plates one day prior to inhibitor treatment. For the experiments, cells were treated with increasing concentrations of inhibitor (0.12 μ M to 30 μ M Rebastinib), (0.004 μ M to 1.11 μ M OSI-906) in normal growth medium and the control condition was treated with a corresponding amount of vehicle (0.1% DMSO). A cell viability assay was performed after 48 h (Rebastinib) or 72h (OSI-906) of treatment using the Cell counting kit 8 (Sigma-Aldrich), according to the instructions of the manufacturer. Absorbance was measured at 450 nm using a FLUOstar Omega microplate reader from BMG Labtech. Measurements were performed in quadruplicates (Rebastinib) or three biological (nine technical) replicates for the OSI-906 experiments for each condition. An IC₅₀ value, corresponding to a concentration yielding a 50% reduction in cell viability was determined using non-linear regression in GraphPad Prism.

Cellular thermal shift assay

Cells were seeded in 15-cm dishes one day prior to the experiment. For experiments, cells were treated with 1.8 μ M of Rebastinib (IC₅₀) or a corresponding amount of DMSO (0.1% DMSO) for 30 min. Cells were collected in PBS, centrifuged and resuspended in PBS with 0.4% NP-40 including protease inhibitors. The cell suspensions were equally distributed into PCR tubes and heated for 4 minutes in a thermocycler (Mastercycler, Eppendorf) at the indicated temperatures (increasing from 37°C to 67°C) before three consecutive snap freeze-thaw cycles using dry ice. Samples were centrifuged (1 h, 20,000xg) and the supernatant was used for immunoblotting against CDK16.

Quantitative Neurite Outgrowth Assay

For quantitative evaluation of neurite outgrowth, SH-SY5Y cells were seeded in complete medium in black 24-well plates (Ibidi) and treated with siRNAs (targeting Cbl and Cbl-b or CDK16), RA, or stimulated with ligands in 0.5% FBS-containing medium (20-100 ng/ml of FGF-2, IGF-1, PDGF-BB or TGF α). Ligands were replenished every 24 hours. For experiments combining siRNA knockdown with chemical inhibition, cells were treated with the indicated concentration of inhibitor (U0126, SHP099 or

Rebastinib), while control cells were incubated with corresponding amounts of DMSO (0.1%). Evaluation of neurite outgrowth was performed 48-72 hours after initiation of the experiment (stimulation or siRNA transfection with/without inhibitor treatment). Prior to image acquisition, nuclei were stained with Hoechst 33342 (Invitrogen/Thermo Fisher Scientific). Visualization and image acquisition were done by live-cell imaging on a ScanR Inverted Microscope high-content screening station (Olympus) equipped with a Hamamatsu Orca flash 4 camera. Images were acquired using a 20x phase contrast objective. Data was acquired by live cell imaging in a closed environmental control system with a humidified atmosphere, CO₂-levels at 5% and temperature-control set to 37°C. Imaging was done in a fully automated fashion using the ScanR acquisition software (Olympus). For each condition, images were acquired on 16 positions each for six replicates, yielding a total of 96 images per condition. Image analysis was done using an in-house developed tool referred to as 'Neurite Outgrowth Quantification'. The tool was developed using *Mathworks* MATLAB version 2018a. This tool enables the automatic segmentation of neurites to extract a measure for the following features: Number of nuclei, area of nuclei and area of neurites.

For basic visualization of neurite outgrowth images were acquired on a phase-contrast microscope (DM1000, Leica) with a DFC420C camera (Leica).

Sample Preparation for Mass Spectrometry Analysis

For all proteomics analyses, cells were washed in PBS and lysed in boiling guanidine-hydrochloride lysis buffer [6 M guanidine-HCl with 100 mM Tris pH8.5, 5 mM tris(2-carboxyethyl)phosphine (TCEP) and 10 mM chloroacetamide]. Collected cell extracts were heated at 99°C for 10 min followed by sonication. Protein concentrations were determined using the Pierce BCA Protein Assay Kit (ThermoFisher Scientific). Proteins were digested with endoproteinase Lys-C for 2-3 hours and diluted to <2 M guanidine-HCl with 25 mM Tris buffer before digestion with trypsin (Sigma-Aldrich) overnight at 37°C. Enzyme activity was quenched by acidification of the samples with trifluoroacetic acid (TFA) and precipitates were removed by centrifugation at 3000 rpm for 5 min. Peptides were purified and concentrated on reversed-phase C18 Sep-Pak cartridges (Waters) and eluted with 40% acetonitrile (ACN) followed by 60% ACN. The eluate was concentrated and acetonitrile removed using a SpeedVac centrifuge, and the peptide concentration was estimated by measuring absorbance at A280 on a NanoDrop (ThermoFisher Scientific).

SILAC-based deep proteome analysis/Offline High pH reversed phase fractionation

For SILAC-based proteome analysis, tryptic peptides were separated and fractionated by high pH (HpH) reversed-phase fractionation using a Waters XBridge BEH130 C18 3.5 μm 4.6 x 250 mm column on an Ultimate 3000 high-pressure liquid chromatography (HPLC) system (Dionex) essentially as described in Batth et al. (Batth et al., 2014) and Bekker-Jensen et al. (Bekker-Jensen et al., 2017). Fractionation was performed at a flow rate of 1 mL/min while constantly introducing 25 mM ammonium bicarbonate (pH8) at 10%. Peptides were separated using a linear gradient of ACN running from 5% to 35% in 62 min, followed by 5 min of 60% ACN before being ramped to 70% ACN for 3 min. For each sample a total of 46 fractions were collected at 90 s intervals using a Dionex AFC-3000 fraction collector. All fractions were acidified by addition of formic acid (FA) to a final concentration of around 0.1% prior to concentration in a SpeedVac centrifuge. The concentration of peptides in each fraction was estimated by measuring absorbance at A280 on a NanoDrop, allowing 1 μg per fraction to be injected for nano-flow liquid chromatography-tandem mass spectrometry (LC-MS/MS).

TMT-labeling and TiO₂-based enrichment of phosphopeptides

Based on the absorbance measurements of SepPak-eluted samples identical amounts of each sample were labeled using TMT10-plex reagents (ThermoFisher Scientific) according to the instructions of the manufacturer. Initially peptide samples were adjusted with ACN to reach a concentration of 50% ACN and with HEPES for a final concentration of approximately 30 mM (pH8). Peptides were labeled for 1 hour using 10 μl TMT-reagent per 100 μg of digested peptide and the reaction was quenched for 15 min with 5% hydroxylamine. Samples were mixed and adjusted with 88% ACN, 12% TFA (to 80% ACN,

12% TFA) for phosphopeptide enrichment with titanium dioxide (TiO₂) beads (GL Sciences) essentially as described in (Jersie-Christensen et al., 2016). Briefly, TiO₂ beads were incubated in a solution of 2,5-dihydrobenzoic acid (DHB) (20 mg/ml, Sigma-Aldrich) in 80% ACN, 1% TFA for 20 min and the bead suspension was added to the adjusted sample (in 1:2 with the amount of labeled peptide) and incubated with rotation for 30 min. After centrifugation the procedure was repeated with the supernatant for a second round of TiO₂-based enrichment. Beads were washed with 80% ACN, 6% TFA followed by 50% ACN, 6% TFA and then 80% ACN, 1% TFA followed by 50% ACN, 1% TFA. The beads were then transferred to C8 StageTips and washed with 10% ACN, 1% TFA followed by 80% ACN, 1% TFA prior to elution with 5% ammonia (NH₄OH) and 10% ammonia (NH₄OH), 25% ACN. Eluted phosphopeptides were concentrated in a SpeedVac centrifuge prior to fractionation. Microflow HPLC reversed-phase fractionation of phosphopeptides was performed on an Ultimate 3000 HPLC system (Dionex) using a Waters Aquity CSH C18 1.7 μm 1 x 150 mm column operating at a constant flow rate of 30 μl/min. The system was equipped with two buffer lines; one containing 5 mM ammonium bicarbonate (pH 8) and one containing 100% ACN. Peptides were separated by a linear gradient of ACN from 5% to 25% over 62.5 min followed by a 4.5 min increase to 60% before being ramped to 70% over 3 min. 12 concatenated fractions were collected per sample. All fractions were acidified by addition of 10% formic acid, SpeedVac'ed to dryness and resolubilized with 80% ACN, 0.1% formic acid. Fractions were then concentrated by SpeedVac and adjusted with 5% ACN, 0.1% TFA prior to MS analysis. TMT proteome samples were handled in a similar manner except for excluding the phosphopeptide enrichment and adding a Sep-Pak purification step in between TMT-labeling and HPLC fractionation.

Sample preparation for MS-based analysis of ubiquitylated peptides

SILAC-based analysis of ubiquitylated peptides was performed essentially as described in (Akimov et al., 2018). Initially cells were washed in PBS and lysed in guanidine-hydrochloride lysis buffer [6 M guanidine-HCl with 100 mM Tris pH8.5], then snap-frozen in liquid nitrogen and stored at -80°C. Cell extracts were sonicated and centrifuged at high speed for 30 min, prior to reduction and alkylation for 30 min at room temperature with 5 mM TCEP and 10 mM chloroacetamide. Protein concentrations were determined using the Pierce BCA Protein Assay Kit (ThermoFisher Scientific) and equal amounts of the two SILAC conditions were mixed for each sample. Samples were diluted to a guanidine-HCl concentration <2 M using 25 mM Tris buffer and filtered through 0.45 μm PVDF filters (Millipore) before overnight digestion with Lys-C (added in 1:100 with protein ratio). Peptides were purified using C18 SepPak cartridges (Waters) and the eluate was lyophilized for 24 to 36 hours. The lyophilized peptides were dissolved in 20-25 mL of IP buffer [50 mM MOPS pH7.5, 50 mM NaCl, 10 mM sodium phosphate] containing 0.1% Triton X-100. The peptide solution was centrifuged and filtered through 0.45 μm PVDF filters prior to incubation with UbiSite-conjugated matrix under rotation for 5 hours at 4°C. Beads were washed three times with IP buffer (not containing detergent) and three times with 150 mM NaCl. Immunoprecipitated peptides were eluted by three sequential rounds of 5 minute incubations with 0.1% TFA. Following elution from the beads the pooled eluate was pH-adjusted using 1 M ammonium bicarbonate (final concentration of approximately 25 mM) and the peptides were digested with trypsin overnight at 37°C. Ubiquitylated peptide mixtures were separated by step-wise high-pH reversed phase fractionation using a C18 StageTip (two C18 discs and 0.5 cm of C18 beads (ReProsil-Pur AQ, Dr Maisch)). The StageTip was activated with methanol and washed once with Buffer B [50% ACN, 5 mM ammonium hydroxide] and twice with Buffer A [10 mM ammonium hydroxide pH10]. Samples were adjusted to 10 mM ammonium hydroxide corresponding to pH10 and loaded onto the StageTip followed by two washes with Buffer A. The samples were fractionated into 16 fractions by sequential elutions with 10 mM ammonium hydroxide containing increasing amounts of ACN, using the following ACN gradient: 1.75%, 2.75%, 3.5%, 4%, 5%, 5.5%, 6%, 7%, 8%, 9%, 10.5%, 12%, 14%, 17.5%, 25% and 50%. All fractions were dried in a SpeedVac, resolubilized with 80% ACN, 0.1% formic acid and then concentrated by SpeedVac and adjusted with 5% ACN, 0.1% TFA prior to MS analysis.

Nanoflow liquid chromatography-tandem mass spectrometry (LC-MS/MS)

All samples were analyzed using an Easy nLC1000 or -1200 (ThermoFisher Scientific) coupled to a Q-Exactive HF mass spectrometer (ThermoFisher Scientific) through a nano electrospray source as described previously (Kelstrup et al., 2014). Peptides were separated on a 15-cm analytical column (75 μ m inner diameter) in-house packed with 1.9 μ m reversed-phase C18 beads (ReProsil-Pur AQ, Dr Maisch) and column temperature was maintained at 40°C by an integrated column oven (PRSO-V1, Sonation GmbH). Each peptide fraction was injected using an autosampler and separated in turn using different gradients depending on the type of sample being analyzed. For SILAC-based proteome analysis, a 30 min gradient ranging from 10% to 30% Buffer B over 25 min to 45% B in the following 5 min and using a flow of 350 nL/min was applied. For SILAC-based analysis of ubiquitylated peptides a 60 min gradient ranging from 5% to 30% Buffer B over 50 min to 45% B in the following 10 min and using a flow of 250 nL/min was applied. For TMT-based phosphoproteome and proteome analysis a 60 min gradient ranging from 10% to 30% Buffer B over 50 min to 45% B in the following 10 min and using a flow of 250 nL/min was applied.

The mass spectrometer was operated in data-dependent acquisition mode with spray voltage at 2 kV, heated capillary temperature at 275°C and s-lens radio frequency level at 50%. Dynamic exclusion was set to 30 s and experiments acquired in positive polarity mode. For every full scan the TopN most intense ions were isolated and fragmented by higher-energy collisional dissociation (HCD) with a normalized collision energy of 28% or 33%.

For SILAC-based proteome analysis full scan resolution was set to 60,000 at m/z 200 and the mass range was set to m/z 350-1400. Full scan ion target value was 3E6 with a maximum fill time of 45 ms. For fastest HCD-MS/MS scanning a Top20 method was applied with fragment scan resolution of 15,000 and an ion target value of 1E5 with a maximum fill time of 15 ms. For SILAC-based analysis of ubiquitylated peptides full scan resolution was set to 60,000 at m/z 200 and the mass range was set to m/z 375-1500. Full scan ion target value was 3E6 with a maximum fill time of 25 ms. For HCD-MS/MS scanning a Top10 method was applied with fragment scan resolution of 45,000 and an ion target value of 2E5 with a maximum fill time of 86 ms. For TMT-based phosphoproteome and proteome analysis full scan resolution was set to 120,000 at m/z 200 and the mass range was set to m/z 400-1600. Full scan ion target value was 3E6 with a maximum fill time of 20 ms. For HCD-MS/MS scanning a Top10 method was applied with fragment scan resolution of 60,000 and an ion target value of 2E5 with a maximum fill time of 110 ms.

Processing and analysis of mass spectrometry raw data

Raw MS data files were analyzed using the MaxQuant software version 1.5.3.36, 1.5.8.4 and 1.6.0.17 with the integrated Andromeda search engine (Cox and Mann, 2008; Cox et al., 2011) and searched against a target/decoy version of the human UniProt database, supplemented with commonly observed contaminants. Cysteine carbamidomethylation was searched as a fixed modification, while protein N-terminal acetylation, oxidized methionine, pyroglutamate formation from glutamine and phosphorylation of serine, threonine and tyrosine were searched as variable modifications for all files. Deamidation of asparagine and glutamine was included as extra variable modification. In addition, ubiquitylation of lysines and N-termini (as GG-remnants), were searched as variable modifications for ubiquitin pulldown samples. Maximum peptide mass was set to 7500 Da. A false discovery rate (FDR) of 1% was applied for identifications on peptide, protein and site level.

Bioinformatic data analysis

Analysis of the proteomics data was performed using Perseus software version 1.5.1.12 or 1.5.2.11 (Tyanova et al., 2016). For TMT 10-plex phosphoproteome and proteome analysis, measured intensities were normalized by quantile-based normalization (Bolstad and Irizarry, 2003) followed by median subtraction within rows. For the TMT phosphoproteome (and proteome) data identified phosphorylation sites/proteins were filtered such that they had to be identified in minimum two replicates for at least one of the sample groups and only sites with a localization probability of at least 0.75 (class I sites) were included in the statistical analysis. Significantly regulated sites and proteins were identified

by ANOVA using a permutation-based FDR of 0.05. For SILAC-based analysis of proteome and ubiquitylome MaxQuant normalized ratios were used. SILAC data were filtered such that a protein or site had to be identified in all of the replicates for at least one of the sample groups in order to be retained in the analysis. For SILAC-based proteome analysis, significantly regulated proteins were identified by ANOVA using a permutation-based FDR of 0.001 and presented with all ratios relative to the siGFP control. Significantly regulated ubiquitin sites were identified by a one-sample t-test using a Benjamini-Hochberg corrected FDR of 0.05. To perform statistical testing for the ubiquitin pulldown the total mean of all ubiquitin site ratios were used. All data were filtered for reversed hits and contaminants. Heatmaps were generated based on unsupervised hierarchical clustering using the Perseus software. GO term enrichment analysis and KEGG pathway enrichment analysis were performed using InnateDb (Lynn et al., 2008). Sequence motif analysis was done using the IceLogo software (Colaert et al., 2009). A sequence motif logo plot of +/- 6 amino acids adjacent to the phosphorylated residue was generated using default parameters with $P < 0.01$. The functional interaction networks and associated GO terms were obtained using STRING and Cytoscape version 3.7.0 (Franceschini et al., 2013; Shannon et al., 2003). For networks with phosphoproteome data different site ratios were collapsed into one common ratio for proteins with more than one regulated phosphosite. The InstantClue software was used for generation of selected figures (Nolte et al., 2018).

Statistical analysis

For experiments with effects indicated as fold changes relative to control, statistical significance was determined by one-sample t-test or one-way ANOVA. For neurite outgrowth experiments data were filtered for outliers using the ROUT method with default parameters in GraphPad Prism. Significance testing was done using either a student's t-test or one-way ANOVA. Results with P-values < 0.05 were deemed as significant.

Supplemental References

- Batth, T.S., Francavilla, C., and Olsen, J.V. (2014). Off-line high-pH reversed-phase fractionation for in-depth phosphoproteomics. *J. Proteome Res.* *13*, 6176–6186.
- Bolstad, B.M., and Irizarry, R.A. (2003). A comparison of normalization methods for high density oligonucleotide array data based on variance and bias. *19*, 185–193.
- Cox, J., and Mann, M. (2008). MaxQuant enables high peptide identification rates, individualized p.p.b.-range mass accuracies and proteome-wide protein quantification. *Nat. Biotechnol.* *26*, 1367–1372.
- Cox, J., Neuhauser, N., Michalski, A., Scheltema, R.A., Olsen, J.V., and Mann, M. (2011). Andromeda: A peptide search engine integrated into the MaxQuant environment. *J. Proteome Res.* *10*, 1794–1805.
- Franceschini, A., Szklarczyk, D., Frankild, S., Kuhn, M., Simonovic, M., Roth, A., Lin, J., Minguez, P., Bork, P., Von Mering, C., et al. (2013). STRING v9.1: Protein-protein interaction networks, with increased coverage and integration. *Nucleic Acids Res.* *41*, 808–815.
- Jersie-Christensen, R.R., Sultan, A., and Olsen, J.V. (2016). Simple and Reproducible Sample Preparation for Single- Shot Phosphoproteomics with High Sensitivity. In *Phospho-Proteomics: Methods and Protocols, Methods in Molecular Biology*, pp. 251–260.
- Kelstrup, C.D., Jersie-Christensen, R.R., Batth, T.S., Arrey, T.N., Kuehn, A., Kellmann, M., and Olsen, J.V. (2014). Rapid and deep proteomes by faster sequencing on a benchtop quadrupole ultra-high-field orbitrap mass spectrometer. *J. Proteome Res.* *13*, 6187–6195.
- Lynn, D.J., Winsor, G.L., Chan, C., Richard, N., Laird, M.R., Barsky, A., Gardy, J.L., Roche, F.M., Chan, T.H.W., Shah, N., et al. (2008). InnateDB: Facilitating systems-level analyses of the mammalian innate immune response. *Mol. Syst. Biol.* *4*.
- Nolte, H., Macvicar, T.D., Tellkamp, F., and Krüger, M. (2018). Instant Clue : A Software Suite for Interactive Data Visualization and Analysis. 6–13.
- Shannon, P., Markiel, A., Ozier, O., Baliga, N.S., Wang, J.T., Ramage, D., Amin, N., Schwikowski, B., and Ideker, T. (2003). Cytoscape: a software environment for integrated models of biomolecular interaction networks. *Genome Res.* *13*, 2498–2504.
- Tyanova, S., Temu, T., Sinitcyn, P., Carlson, A., Hein, M.Y., Geiger, T., Mann, M., and Cox, J. (2016). The Perseus computational platform for comprehensive analysis of (prote)omics data. *Nat. Methods* *13*, 731-740.